The Optical Model Spectral Validation and Annual Water Clarity Reporting Tool: Final Report

L. Kellie Dixon[1] and Michael R. Wessel[2]

1 - Mote Marine Laboratory
1600 Ken Thompson Parkway
Sarasota, FL 34236

2 – Janicki Environmental, Inc.
1155 Eden Isle Dr. NE
St. Petersburg, FL 33704

July 30, 2014
Mote Marine Laboratory Technical Report No. 1748

EXECUTIVE SUMMARY

A spectrally explicit empirical optical model was developed and calibrated for all 14 Charlotte Harbor seagrass management segments to estimate the diffuse attenuation coefficient, K_{dPAR}, at the target depths previously identified by the Charlotte Harbor National Estuary Program (CHNEP). The model was calibrated using specialized data collected in 1997-1998, as well as an optimized subset of data collected from the routine CHNEP water quality monitoring network of estuarine waters with measured values of color, chlorophyll, turbidity, and field K_{dPAR} values. The model accounts for sun angle, and computes absorption, and scattering components of light attenuation through the water column in terms of the water quality constituents. The model simulates regionally- and spectrally-explicit partial attenuation coefficients for wavelengths between 400 and 700nm, estimating both overall water clarity and the light available at seagrass target depths.

Calibration statistics indicated that modeled K_{dPAR} demonstrated excellent agreement with observed K_{dPAR} within the range of target depths and water quality conditions relevant to the success of seagrasses in CHNEP estuarine waters. Comparison of modeled and observed K_{dPAR} produced an intercept of -0.003 m^{-1} and a slope of 0.98 (relative to an expected range of 0.8-1.2, and an ideal of 1.0). The median root mean square error was 0.15 m^{-1} and median residuals by segment were less than 0.24 m^{-1} (the K_d of water alone), indicating a robust model.

The calibrated optical model represents a quantifiable method of evaluating water clarity for all Charlotte Harbor segments based on grab sample water quality data without having to measure light in the field. The resulting predicted K_{dPAR} values from the spectrally explicit optical model were used to generate annual water clarity scores similar to the previously developed CHNEP Water Clarity Reporting Tool. The scores are computed relative to a reference period (2003-2007) from the data collected under the CHNEP probabilistic water quality monitoring network design. Comparison of selected percentiles (30^{th} and 70^{th}) of individual years to the reference period percentiles permitted the assessment of increased or decreased modeled water clarity. Overall scores of clarity change were computed and categorized based on whether a segment had been designated as a seagrass “Protection” or a “Restoration” target. This provided a mechanism for the spectrally explicit model results and year to year trends in water clarity to be conveniently conveyed to the general public. Comparisons of future scores to the reference period remain valid only as long as the design frequency and spatial density of the monitoring program remains essentially the same as during which the reference values were developed.

The calibrated model predicts light attenuation of optically deep conditions (i.e. no bottom reflectance), at solar noon, under the assumption of direct sunlight only (i.e. no diffuse skylight from the portion of the hemisphere other than the sun itself), under calm conditions and does not directly capture the within-day variability in light attenuation due to wave height, fetch, overcast conditions, solar angle, and bottom reflectance. The model responds to changes in water column attenuating substances only, rather than to clarity changes produced by changing illumination conditions. As a result, the modeled values are considered to be a more reliable indicator of the long term water clarity conditions than field observed light data given the

complexities and potential measurement error associated with measuring light in the very shallow estuarine waters of the CHNEP.

Future efforts to assess the optical properties of the CHNEP estuarine waters should focus on understanding the role of mineral suspended particulates in the scattering component of light attenuation as a result of onshore winds and beach resuspension. Additional absorption measurements on samples of this type would allow particulate absorption to be fit to a "typical" particle type and may improve the residuals in segments with access to the Gulf of Mexico. The types of particles could be further distinguished by total suspended solids (TSS) and volatile suspended solids (VSS) analyses, but model recalibration would need to be conducted to take advantage of the new analyses, and TSS and VSS would need to be incorporated into the CCHMN in the future. The lack of PAR observations at more than two depths in Dona and Roberts Bays and Upper Lemon Bay limited the restrictions that could be placed on field K_{dPAR} data to ensure that the highest quality observations were used for model calibration but residuals compared with segments in which multi-depth observations were made indicated no significant biases imposed due to the two depth observations. Investigations of laboratory data and methods for spectrophotometric color would be helpful to confirm to confirm the variation in conversion of color in PCU determined at 465 nm to a_{g440}.

The Annual Water Clarity Reporting Tool should also be re-evaluated periodically in future years once sufficient data are available to correlate the scores with the areal extent of seagrass changes. Examining individual scores from the 30^{th} and 70^{th} percentile would allow for independent assessments of how changes in the distribution of modeled water clarity is associated with changes in seagrass acreage. Together, the Optical Model and the Annual Water Clarity Reporting Tool represent an important step forward for the CHNEP to collect and disseminate information relevant to a keystone indicator of estuarine condition in CHNEP estuarine waters and to optimize the sampling and reporting of estuarine conditions to the CHNEP constituents.

ACKNOWLEDGMENTS

The Charlotte Harbor National Estuary Program is a partnership of citizens, elected officials, resource managers and commercial and recreational resource users working to improve the water quality and ecological integrity of the greater Charlotte Harbor watershed. A cooperative decision-making process is used within the program to address diverse resource management concerns in the 4,400 square mile study area. Many of these partners also financially support the Program, which, in turn, affords the Program opportunities to fund projects such as this. The entities that have financially supported the program include the following:

U.S. Environmental Protection Agency,
Southwest Florida Water Management District,
South Florida Water Management District,
Florida Department of Environmental Protection,
Florida Coastal Zone Management Program,
Peace River/Manasota Regional Water Supply Authority,
Polk, Sarasota, Manatee, Lee, Charlotte, DeSoto, and Hardee Counties,
Cities of Sanibel, Cape Coral, Fort Myers, Punta Gorda, North Port, Venice,
Fort Myers Beach, and Winter Haven,
and the Southwest Florida Regional Planning Council.

We wish to express our appreciation for the long term and continuing efforts of the samplers, analytical staff, funding agencies, and all participants in the Coastal Charlotte Harbor Monitoring Network, whose data made this project possible and to Ms. Bridgette Froeschke for assistance with coding.

TABLE OF CONTENTS

LIST OF FIGURES

LIST OF TABLES

1.0 INTRODUCTION

Purpose

The Charlotte Harbor National Estuary Program (CHNEP) employs objective, science-based, decision making tools for use as indicators of estuarine health. The CHNEP is furthering its goals under the Comprehensive Conservation and Management Plan (CCMP) to protect and restore water quality through rigorous analysis of management tools. The extent of seagrass in the CHNEP study area is an exceptionally valuable natural resource and a primary focus of the CHNEP CCMP. The continued focus on science-based management tools for seagrass will help to ensure the protection of these vital resources as anthropogenic pressures increase.

The purpose of the Charlotte Harbor National Estuary Program Optical Model Spectral Validation and Annual Water Clarity Reporting Tool Refinement Project was to provide the CHNEP with an empirical optical model in which diffuse attenuation coefficients of photosynthetically active radiation or PAR (K_{dPAR}) could be reproducibly computed from the water quality monitoring parameters of color or colored dissolved organic matter (CDOM), chlorophyll *a,* and turbidity. The model was to be calibrated against field measurements of K_{dPAR} made in each segment of the CHNEP study area. The calibrated model was then to be applied the entire body of water quality monitoring data to estimate annual water clarity conditions for each of the estuary segments, evaluate modeled water clarity with respect to a designated reference period, and to assess the trends in modeled water clarity over time. The calibrated optical model was to be made available to the Program to share with scientists and the public, specifically via the CHNEP Water Atlas.

Context

Charlotte Harbor is located in southwest Florida and the CHNEP is 1 of 28 National Estuary Programs nationwide established to implement the federal Clean Water Act. CHNEP activities are guided by the Comprehensive Conservation and Management Plan (CHNEP, 2008) which addresses Priority Problems, Quantifiable Objectives, and Priority Actions in order to accomplish the Program goals. The project addressed the following CCMP Priority Actions:

- **WQ-B:** Identify gaps in water quality data needed to calibrate models used to assess impairments.
- **WQ-G:** Develop site-specific criteria for dissolved oxygen, chlorophyll *a*, turbidity, salinity and pesticides as applicable.
- **FW-F**: Restore and protect a balance of native plant and animal communities.
- **SG-3**: By 2010, the program for long-term monitoring strategy and management strategy will be implemented and resulting informational websites maintained systematically.
- **SG-R**: Track and present monitoring data according to CHNEP adopted targets in Environmental Indicators.
- **SG-S:** Post raw data, geographic information system and technical analysis on the Internet under the data management strategy.

- **SG-D:** Produce watershed and estuary communication tools.
- **SG-K:** Present scientific information in a form readily understood by the majority of people.
- The Project also addressed several Environmental Indicators relating to status and trends in water quality (WQ-b, WQ-c) and seagrass (FW-a, FW-b) conditions.

Background

The greater Charlotte Harbor watershed includes all or parts of Lee, Charlotte, Sarasota, Manatee, Polk, Hardee and DeSoto Counties and contains three major rivers: the Myakka, Peace and Caloosahatchee Rivers. The estuarine portion has been divided into segments of relatively homogeneous seagrass and water quality conditions (Figure 1). The most recent recommended segmentation scheme (JEI, 2009a) includes Upper Lemon Bay, Lower Lemon Bay, Tidal Myakka River, Tidal Peace River, East Wall, West Wall, Bokeelia (also known as Lower Charlotte Harbor), Cape Haze, Pine Island Sound, Matlacha Pass, Tidal Caloosahatchee River, San Carlos Bay and Estero Bay. Dona and Roberts Bays, at the northern end of the study area, has also been included in subsequent work, for a total of 14 named divisions

In 2006, CHNEP adopted initial water clarity targets (Corbett and Hale, 2006; Corbett, 2006). Target seagrass depths were established for estuary segments based on the maximum of either the observed maximum annual mean depths of 1999-2005 seagrass transects or the 95^{th} %-ile of seagrass depth distributions in 2003. Literature-derived seagrass light requirements were assumed to be 25% (Tomasko and Hall, 1999; Dixon, 2000; Tomasko and Hall, 1999; Greening and Janicki, 2006) of immediately subsurface photosynthetically active radiation (PAR) and target K_{dPAR} values were computed from target depths and 25% PAR.

In 2009, CHNEP initiated a refinement of the water quality targets. Seagrass acreage targets were established (Janicki, et al., 2009) as the greater of either the 1950's baseline acreage (adjusted for non-restorable areas) or the mean of all recent seagrass surveys from 1988, 1994, 1999, 2001, 2004, and 2006. Segments were designated for "Restoration" when recent acreages were less than adjusted baseline and for "Protection" when recent acreages were greater than baseline. No seagrass management targets were established for the tidal riverine segments due to the difficulty interpreting aerial photography in high color systems (Dona and Roberts Bays, Tidal Myakka, Tidal Peace, and Tidal Caloosahatchee Rivers). However, the segments with high color were assigned a "Protection" or "Restoration" designation based on regulatory status and local expertise (JEI, 2011). Some minor revisions to the depth targets of Corbett (2006) were also made in these segments.

The seagrass target depths, together with a 25% PAR requirement, allowed the computation of segment-specific light attenuation coefficients, K_{dPAR} (Table 1), as water clarity targets. Comparisons of clarity targets with measured K_{dPAR} values were puzzling, however, in that measured K_{dPAR} generally exceeded clarity targets (JEI, 2010). Values of K_{dPAR} modeled with the partial attenuation coefficient approach (McPherson and Miller, 1987; Corbett, 2006; JEI, 2010) were also high, particularly for K_{dPAR} less than 1.0-1.5 m^{-1}. Water clarity targets were

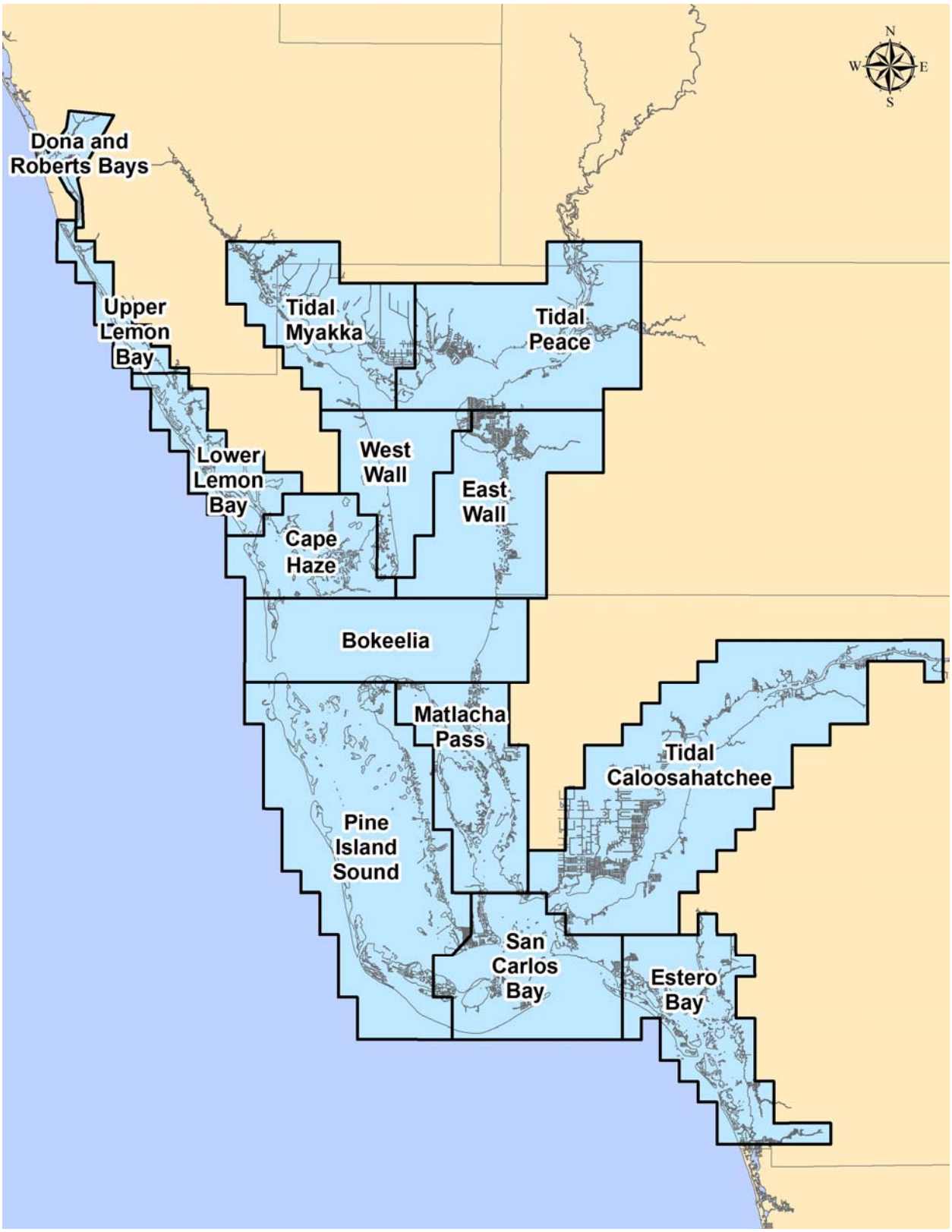

Figure 1. Seagrass management and optical modeling segments.

Table 1. Seagrass segments, target depths, and K_{dPAR} required for 25% PAR at target depths. Restoration segments in blue.

Segment	Abbrev.	Target Depth (m)	Target Kd for 25% PAR (m^{-1})
Dona and Roberts Bays*	DRB	1	1.39
Upper Lemon Bay	ULB	2	0.69
Lower Lemon Bay	LLB	2	0.69
Tidal Myakka River*	TMR	0.9	1.54
Tidal Peace River*	TPR	1	1.39
West Wall	WW	1.4	0.99
East Wall	EW	1.4	0.99
Cape Haze	CHZ	1.9	0.73
Bokeelia	BOK	2.4	0.58
Pine Island Sound	PIS	2.2	0.63
Matlacha Pass	MP	2	0.69
San Carlos Bay	SCB	2.2	0.63
Tidal Caloosahatchee River*	TCR	1	1.39
Estero Bay	EB	1.6	0.87

* - No management target

subsequently established based on observed water clarity data for the reference period (2003 – 2007) by using cumulative frequency distribution curves and selected percentiles of observed light attenuation values (JEI, 2010). Progress over time towards meeting water clarity targets has been evaluated using the Annual Water Clarity Reporting Tool (JEI, 2011) as applied to measured attenuation coefficients. The Tool generated annual water clarity scores for each of the estuary segments based on the percentage of water clarity measurements that were better or worse than the target percentiles for a given year.

These and subsequent analyses have shown that there was a lack of statically rigorous relationships between water clarity estimates from field measurements of light attenuation and empirical partial attenuation coefficient model results (Wessel and Corbett, 2009; JEI, 2010). More recent research (Dixon et al., 2010) indicated that empirical, spectrally-explicit optical models using water quality data (CDOM, chlorophyll *a* and turbidity) may more consistently represent water clarity conditions than actual field measurements of light attenuation. In addition, a properly validated empirical optical model could be applied to past water quality data available prior to when light attenuation measurements were collected, and could minimize time in the field.

Therefore, a spectrally–explicit optical model was to be developed for the study area to predict water clarity from all available water quality data (CDOM, chlorophyll *a* and turbidity) and to estimate annual water clarity conditions for each of the estuary segments. The distribution of the updated modeled water clarity estimates was also to be used to update the Water Clarity

Reporting Tool and to provide a readily understood format for sharing progress towards meeting water clarity and seagrass targets. In addition, the validated optical model was to be made available to the CHNEP to share with scientists and the public, specifically via the CHNEP Water Atlas.

1.1 MODEL DESCRIPTION

The empirical optical model originated with equations presented in Kirk (1981, 1984, 1991, 1994) and Gallegos (1993) in which the vertical diffuse attenuation coefficient for a given wavelength ($K_{d\lambda}$) is a function of solar zenith angle (the cosine of the angle of the sun from vertical or μ_0), and wavelength-specific scattering (b) and total absorption (a_t) coefficients.

$$K_{d\lambda} = \frac{1}{\mu_0} [a_t^2 + (g_1 * \mu_0 - g_2) * a_t * b]^{1/2} \quad (1)$$

The coefficients g_1 and g_2 are numeric constants, empirically determined for the midpoint of the euphotic zone (Kirk, 1994). Models are regionally calibrated to obtain the inherent optical properties (IOP) of a_t and b numerically described in terms of monitoring water quality data. The resultant model incorporates the characteristic spectral properties of local colored dissolved organic matter (CDOM) or *gelbstoff*, the pigments of typical phytoplankton communities, and the absorption and scattering properties of typical suspended material. The model returns a wavelength-specific (2 nm increments) vertical diffuse attenuation coefficient of an optically deep water column, under standardized conditions, and for the specified water quality conditions of color, chlorophyll, and turbidity.

Empirical model outputs retain the assumptions under which they were formulated and calibrated. The model simulates $K_{d\lambda}$ under optically deep conditions (i.e. no bottom reflectance) and under direct sunlight only (i.e. direct radiance from the solar disk and not including irradiance due to scattered light or skylight from the remaining portion of the hemisphere). Light from bottom reflectance which "contaminates" the PAR readings of a lower sensor (particularly spherical or 4π sensors) would tend to decrease observed K_{dPAR} measurements relative to modeled values. Larger proportions of diffuse light (as during low sun angles or under overcast conditions) by entering the water column at larger zenith angles and having a longer path length for absorption before reaching a specified depth, would result in increases in observed values of K_{dPAR} relative to modeled values.

Literature values of the spectral distribution of incident irradiance, adjusted for seasonal earth-sun distance and time-of-day atmospheric attenuation, and modeled $K_{d\lambda}$ are then used to compute spectral irradiance at a selected depth (z). Irradiance values are integrated over the spectra (400-700 nm) to obtain total PAR just below the surface (I_0) and at depth z (I_z), and used to compute the %PAR at depth and the K_{dPAR} as:

$$\%PAR = (I_z / I_0) * 100\% \quad (2)$$

$$K_{dPAR} = - ln (I_z / I_0) / z \quad (3)$$

Modeled K_{dPAR} can then be compared with K_{dPAR} field measurements made with a PAR quantum meter which responds similarly to all wavelengths of light (LiCOR or equivalent) for calibration. Due to the variation in K_d with wavelength, and the differential attenuation of various wavelengths, the K_{dPAR} computed is strictly applicable only to the depths between which it was derived. Modeled K_{dPAR} can decrease by 10-20% between 0.5 and 2.0 m, requiring model calibration at the same depths as field observations were made.

The actual time of field measurements and resulting sun angle are used when calibrating the model, but modeling for trend assessment will be conducted using simulations at local noon on the date of the water quality sample collection. The use of the standardized conditions and local noon produce light values at depth that can be considered a daily maxima for the given water quality parameters and direct sunlight assumptions. Modeled data are consequently unaffected by time of day, cloud cover, and bottom type, responding only to water column attenuators.

The empirical model approach has been repeatedly validated and used under a wide range of water quality conditions (Kirk, 1981; 1984; 1991; 1994b; Gallegos, 1993; 1994; 2001; 2005; Gallegos et al., 1990; 2006; Johansson, 2007; 2012; Johansson et al., 2009; Dixon and Kirkpatrick, 1999; Biber et al., 2008; Dixon et al., 2010; Dixon, 2014). Models based on the solution of radiative transfer equations (Mobley, 1994) have also been used to validate the spectral empirical models (Gallegos, 2001), resulting in very high and unbiased correlations between the two approaches in optically deep areas. The agreement between empirical and radiative transfer models results further implies that the source of scatter between observed and empirically model K_{dPAR} values should be attributed to conditions not modeled (optically shallow systems, skylight) or the difficulty of making K_{dPAR} measurements rather than to any bias in the empirical modeling approach.

2.0 MODEL DEVELOPMENT

2.1 MODEL CALIBRATION DATA

For the application of the Annual Water Clarity Reporting Tool, a time series of color, chlorophyll, and turbidity data were required at spatially and temporally representative stations, with a similar sampling design to that employed during the reference period of 2003-2007. For calibration of the optical model, a database of concurrently collected date, time, color, chlorophyll, turbidity, and K_{dPAR} was required. For model formulation, specialized data of concurrent chlorophyll, color, and turbidity, together with spectral absorption scans of dissolved, particulate and de-pigmented particulates were needed.

Overall water quality data for use with the Water Clarity Reporting Tool (electronic Appendix A; DATA_WQ) were compiled for the 14 segments by appending data to selected parameters of

the Task 5 database approved in March 2010, resulting in data updated through December 2011 for random stations sampled under the Charlotte Harbor Monitoring Network. (Dona and Roberts Bays and Upper Lemon Bay programs sample only fixed stations although stations were randomized by month and considered random for the purposes of applying the Water Clarity Reporting Tool.) Data updates were also obtained from the respective monitoring network participants for fixed stations. The overall data were censored to those with only complete records of color, chlorophyll, and turbidity (n=13,232). Maximum water quality values recorded were 420 µg L^{-1} Chlorophyll *a*, corrected for pheophytin, 68 NTU of turbidity, 375 PCU of spectrophotometric true color, and 507 PCU of visually determined apparent color.

Differences in the analytical methods for the determination of color were investigated and, despite varying reporting precision between laboratories, it was confirmed that visual determination of apparent color (unfiltered samples) was performed by most entities. Lee County and the South Florida Water Management District (SFWMD), however, performed color by the spectrophotometric absorption of filtered samples at 465 nm relative to Platinum Cobalt Standards. The dominant chlorophyll data available was chlorophyll *a*, corrected or adjusted for pheophytin which was selected for model calibration. Turbidity methodologies were apparently uniform.

For attenuation coefficient data, methodologies have varied over the years and sensor style also varies between collecting agencies. Lee County utilizes spherical or 4π PAR sensors, while the remainder employ the flat, cosine-corrected, or 2π sensors. Experience elsewhere in Southwest Florida estuaries (Dixon and Kirkpatrick, 1995) and literature (Kirk, 1994) indicate that K_d determined with 2π sensors is approximately equal to attenuation of scalar irradiance (K_0, determined with 4π sensors) and so no distinction between sensors was made. Equipment has also variously included a single submersible sensor and an air sensor, or dual submersible sensors with and without air sensors. While a minimum of two submersed observations are required, some techniques record only a single simultaneous pair of readings, while others make observations at multiple depths, or multiple pairs of observations at multiple depths.

For a consistent treatment and to identify outliers, the unprocessed PAR data were obtained from the sampling agencies. Eliminating data that were recorded at depths of 0.0 m, "raw" K_d values were computed as the negative slope of natural log transformed irradiance (or scalar irradiance) values as a function of measurement depth. The r^2 values of these linear relationships were also computed to assess measurement quality. Where a single sensor made multiple observations, individual readings also required correction for changing incident irradiance, resulting in air-corrected values of K_d. Where paired sensors were used to collect a single pair of simultaneous readings at two depths, the incident irradiance conditions were assumed to be identical and air-corrected K_d values were equivalent with raw K_d values. Where multiple pairs of PAR readings were obtained at multiple depths, air correction was required. More recent K_d measurement techniques included a cross calibration of sensors to account for variations between sensors on paired-sensor techniques. The r^2 values of K_d computed from air-corrected and cross-calibrated readings, however, were not significantly different from

those computed with air-corrected data alone, and so no further cross-calibration of sensors was applied.

Air-corrected attenuation coefficient data were merged with water quality data to produce a calibration data set. Where water quality parameters from multiple depths at a station and date were available, water column averages were prepared to link with field K_{dPAR} values. Time series of calibration data were examined graphically by segment and revealed a period between October 2006 and May 2008 when numerous air-corrected K_d values were substantially less than 0.24 m^{-1}, the modeled value for pure water with 0.0 concentrations of color, chlorophyll, and turbidity. The period of reduced K_d did not coincide with reduced levels of water quality parameters and so was attributed to K_d measurement technique and removed from the calibration data. More isolated instances of $K_d < 0.24$ m^{-1} were similarly observed throughout the calibration data, but were censored on a case-by-case basis. Outliers to the broad relationship of color as a function of salinity were also removed resulting in n=6626 (electronic Appendix B; DATA_CAL).

For initial model calibration, data were also restricted to the r^2 associated with computed K_d to be greater than 0.95 and less than 1.0 (i.e. more than 2 data points) and for the r^2 associated with air-corrected K_d to be greater than or equal to the r^2 of "raw" K_d. These restrictions limited the calibration data to 1005 observations of the highest confidence, but also resulted in some segments (DRB, ULB) with no observations in the initial calibration data due to measurement techniques. Maximum water quality values of the model calibration data were 300 PCU of visual color, 260 PCU of spectrophotometric color, 130 µg L^{-1} of chlorophyll *a*, and 23.8 NTU of turbidity.

2.2 ABSORPTION

To formulate the optical model in terms of water quality monitoring parameters, total absorption (a_t) was partitioned into that attributable to water (a_w), chlorophyll or phytoplankton (a_{ph}), detritus (a_d), and dissolved color or gelbstoff (a_g) with an implicit non-linear wavelength dependence of each term:

$$a_t = a_w + a_{ph} + a_d + a_g \qquad (4)$$

Literature values or specialized data sets were used to permit the calculation of spectral partial attenuation coefficients as a function of typical water quality monitoring parameters. Water absorption profiles (a_w) were drawn from literature values (Pope and Fry, 1997). Values, supplied every 2.5 nm, were splined (Matlab 6.R12) to the 2 nm increments desired (Appendix C, Table C-1)

Absorption due to chlorophyll pigment and detritus was determined through the filter pad method of Kishino (1985), Butler (1962), and Cleveland and Weidemann (1993). Samples were collected monthly from eight stations in TMR, TPR, EW, WW, CHZ, and LCH between April 1997 and March 1998 and from an additional four stations in MP, PIS, and SCB between June and

November 1997 for a total of n=137 (Dixon and Kirkpatrick, 1999). Measured volumes of water were filtered through glass fiber filters, scanned for absorbance relative to a clean filter, extracted with methanol to remove pigments, and rescanned. The difference between pre- and post-solvent absorbance was that due to pigments alone and was subsequently corrected for filter diameter, volume filtered, and theoretical path amplification (Beta or β; Bricaud and Stramski 1990; Nelson and Robertson 1993). Absorption coefficients are enhanced by path amplification factors (*Beta*) as result of the increased scatter and additional opportunities for absorption as light transits through the filter pad. Factors can be either a fixed or absorption dependent quantity, vary by particle size or phytoplankton species, and can vary by a factor of 6 or more (Mueller et al., 2003). As no path amplification data were available specific to Charlotte Harbor particulates, path amplification factors were adjusted to optimize modeled K_{dPAR} results with field observations.

The spectral absorption profiles of chlorophyll are typically normalized to absorption at 440 nm, a mean absorption spectra computed from all normalized spectra, and then chlorophyll-specific absorption at 440 nm (a^*_{ph440}) computed via regression as a function of chlorophyll content determined spectrophotometrically or fluorometrically (APHA, 2005; Arar and Collins, 1997). Normalized spectra, however, displayed considerable variation (Figure 2). The variation, particularly in the 550-650 nm range, proved to be seasonal, with samples from the same month grouping together (not shown), which would not captured by this technique.

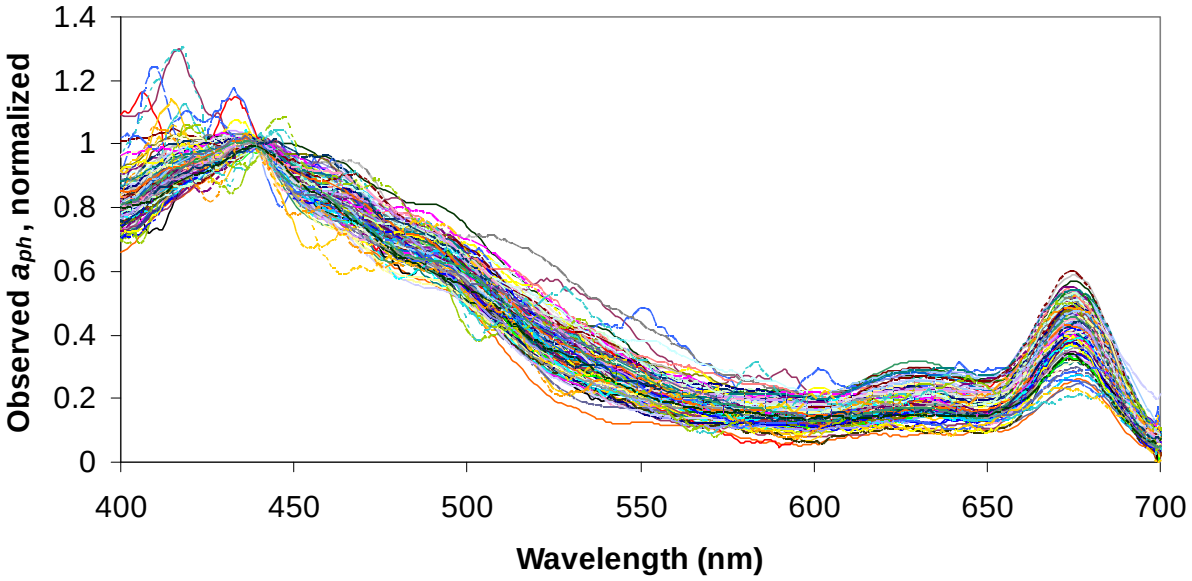

Figure 2. Chlorophyll absorption data from all Charlotte Harbor samples, normalized to a_{ph440} indicating remaining variation.

Accordingly chlorophyll absorption for each wavelength was directly modeled as a series of power relationships of chlorophyll (Figure 3). Coefficient of determinations, r^2, were generally

0.9 or above. The modeled chlorophyll absorption, although less variable than that of the original data, did maintain some portion of the seasonal variation in normalized absorption profiles (Figure 4) with fits substantially improved in the low absorption region of >500 nm. The formulae for a_{ph} were developed with chlorophyll values as high as 143 µg L^{-1}, relative to a maximum of 420 µg L^{-1} in the data to be modeled. Derived coefficients appear in Appendix C, Table C-2. A *Beta* factor for the adjustment of path amplification was empirically derived as 1.8 to optimize the fit between modeled and observed K_{dPAR} over the entire range of the calibration data as a function of chlorophyll alone, resulting in:

$$a_{ph} = C * Chl^{B} \quad (5)$$

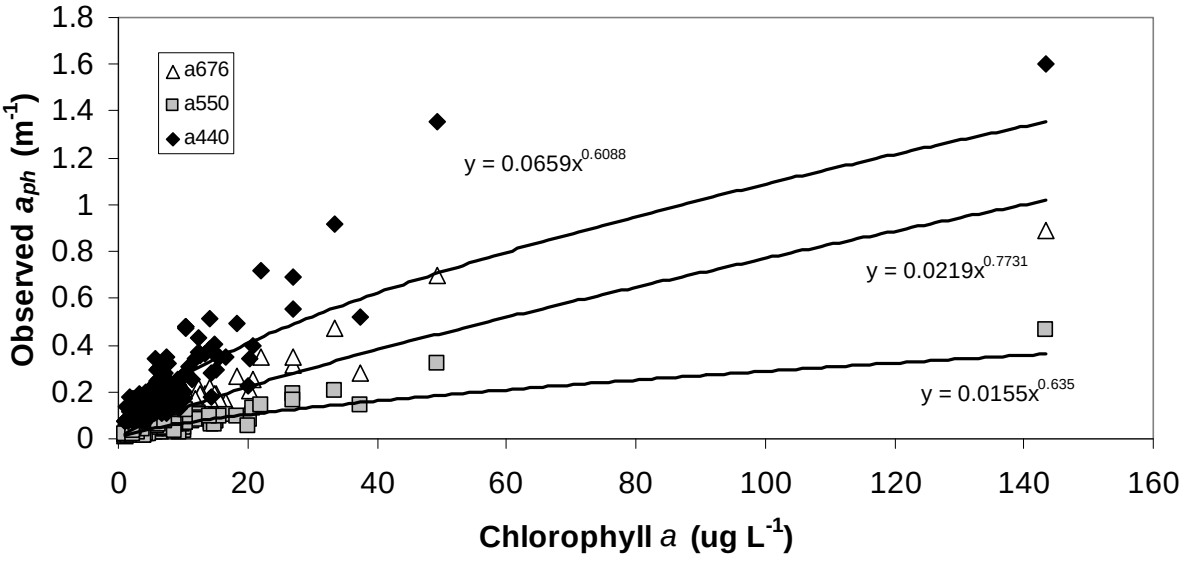

Figure 3. Example of the direct model of chlorophyll absorption, a_{ph}, as derived for wavelengths of 440, 550, and 676.

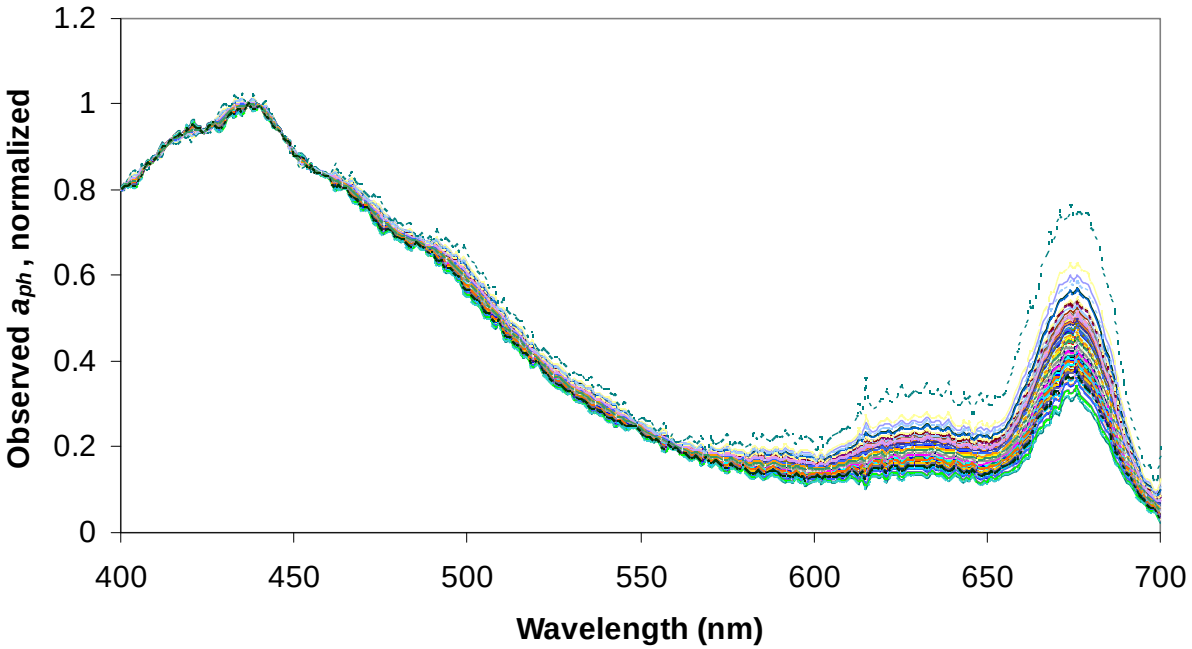

Figure 4. Modeled chlorophyll absorption, a_{ph}, normalized to a_{ph440}

Absorption coefficients due to detritus (a_d) were obtained from the post-solvent extraction scans described above (n=129). Detrital absorption includes not only that due to suspended mineral and organic detrital particles, but also that due to the remaining structural components of de-pigmented phytoplankton. A negative exponential function (Figure 5) very similar to that of CDOM, a_d is generally computed using a reference value at low wavelengths where absorption is maximized. However, examination of a spectral K_d produced with typical values for color, chlorophyll and turbidity indicated that minimum $K_{d\lambda}$ values and maximum resulting %PAR would be mid spectra, in the 500-600 nm region. A residual of ± 0.1 m^{-1} between modeled and observed K_d at high K_d may represent only ± 0.2 %PAR while the same residual can represent ±5 %PAR at low K_d. As the exponential fit to spectral a_d can be imperfect in some regions, the wavelength of the reference a_d (550 nm) and the spectral range of derived slopes (S_d, 500-600 nm) was selected to maximize the fit between modeled and observed a_d in the mid-spectral region.

Minimum values of a_{d550} were established at 0.0 m^{-1}. Spectral slopes, S_d, exhibited a shallow linear slope with a_{g440} (Figure 6), The a_{g440} or CDOM dependence of spectral slope and a_{d550} indicated that precipitated humic and fulvic acids (components of CDOM) likely form the basis of much of the turbidity in the Charlotte Harbor system. A *Beta* path amplification factor of 1.6 was derived by optimizing modeled residuals with respect to turbidity. Maximum turbidity data and a_{g440} data used to develop the empirical formula of a_d were 16.9 NTU and 10.5 m^{-1}, respectively, relative to 68 NTU and 33.7 m^{-1} in the data set to be modeled.

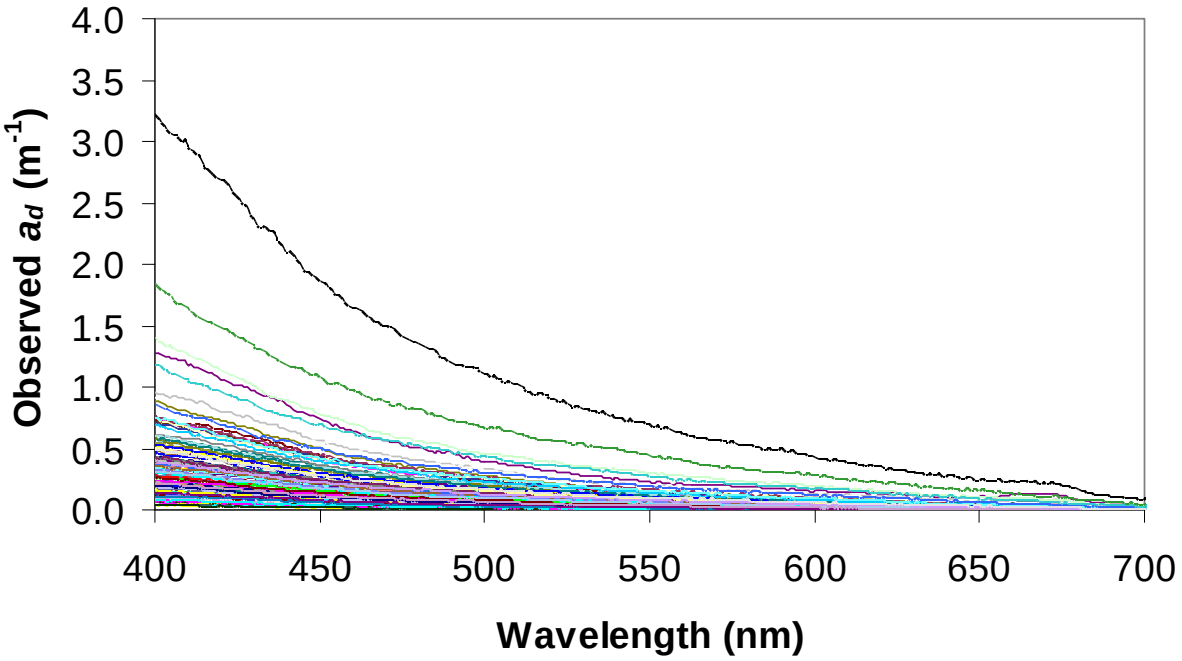

Figure 5. Absorption profiles of de-pigmented phytoplankton, detrital, and mineral particulates, a_d

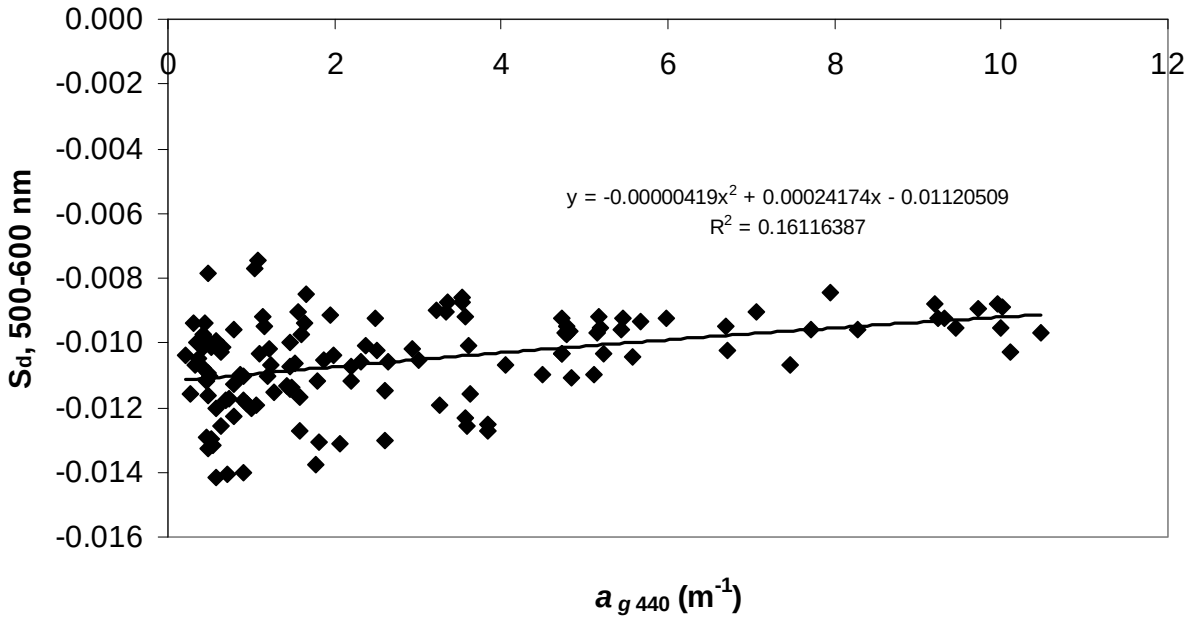

Figure 6. Spectral slope of a_d, S_d, 500-600nm, as a function of a_{g440}

$$a_d = a_{d550} * e^{[Sd * (\lambda - 550)]} \quad (6)$$

$$a_{d550} = \text{MAX}(0, -0.037345 + 0.026239 * \text{Turbidity} + 0.012644 * a_{g440}) \quad (7)$$

$$S_d = -0.00000419 * (1.5 * a_{g440})^2 + 0.00024174 * 1.5 * a_{g440} - 0.01120509 \quad (8)$$

Spectral scans for CDOM or a_g were performed on 138 samples collected in 1997-1998. Samples were filtered through 0.2 micron filters and absorption scans were zeroed at 700 nm where thermal artifacts are minimal and CDOM absorption expected to be absent. Continuing to maximize model accuracy in the region of low overall attenuation, modeled a_g was formulated as a negative exponential function (Bricaud et al., 1981) of reference a_{g500} as:

$$a_g = a_{g550} * e^{[Sg * (\lambda - 550)]} \quad (9)$$

Computing a_{g550} from reported color (PCU) values, however, was dependent on the method of color analysis. Spectrophotometric color (based on absorption at 465 nm) was back transformed from PCU to the a_{g465} of platinum cobalt standards as:

$$a_{g465} = \text{Color}_{\text{PCU-465}} / 16.02895 \quad (10)$$

The resulting a_{g465} of samples was converted to a_{g440} based on the relationship of a_{g465} and a_{g440} (Figure 7) in the 1997-1998 samples of:

$$a_{g440} = 1.58595463 * a_{g465}^{0.95895333} \quad (11)$$

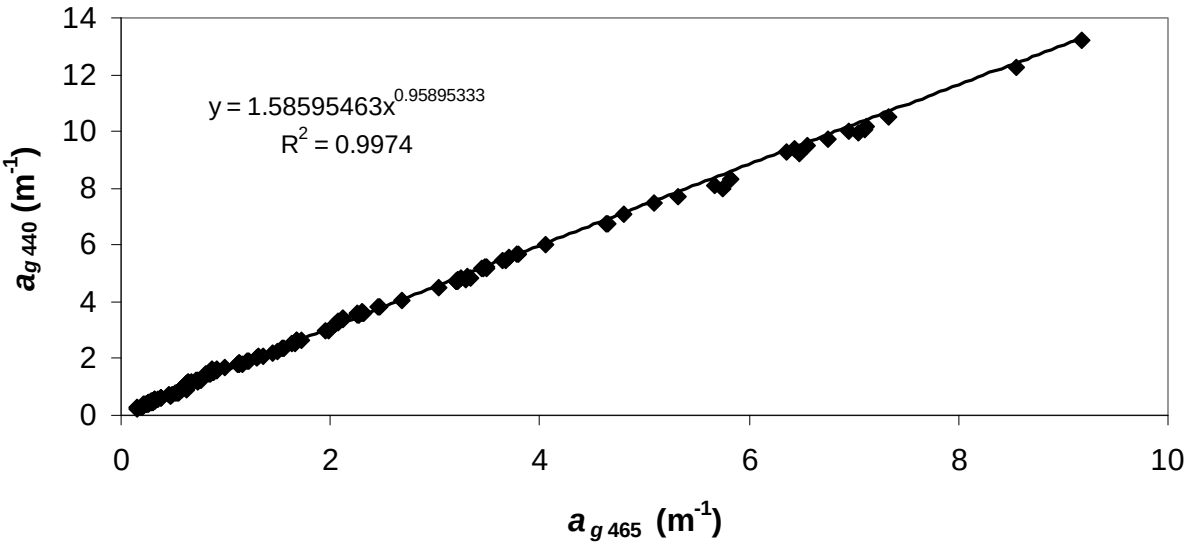

Figure 7. Observed a_{g465} as a function of observed a_{g440}

Apparent color determined visually was converted to a_{g440} based on the visual color determinations of the 1997-1998 samples and the measured a_{g440} (Figure 8).

$$a_{g440} = 0.02842795 * \text{Color}_{\text{PCU-Vis}}^{1.18483956} \quad (12)$$

Subsequently, a_{g550} was computed from either type of derived a_{g440} (Figure 9) as :

$$a_{g550} = \text{MAX}(0, 0.00771348 * (1.5*a_{g440})^2 + 0.16458477* 1.5 * a_{g440} - 0.01053129) \quad (13)$$

Spectral slopes, S_g, of CDOM were determined on *ln*-transformed a_g data between 500-600 nm and modeled as a function of a_{g440}. The function was complex (Figure 10) and was fit as a three part equation to mimic observed slopes and to reasonably account for slopes at a_{g440} higher than observed in the calibration data.

S_g = (14)

If a_{g440} <=4.0,

$0.00040224 * a_{g440}^2 - 0.00232357 * a_{g440} - 0.01267477$

If a_{g440} > 4.0 and a_{g500} <= 13.5,

$-0.00002682 * a_{g440}^2 + 0.00087068 * a_{g440} - 0.01882298$

If a_{g440} > 13.5

-0.01177

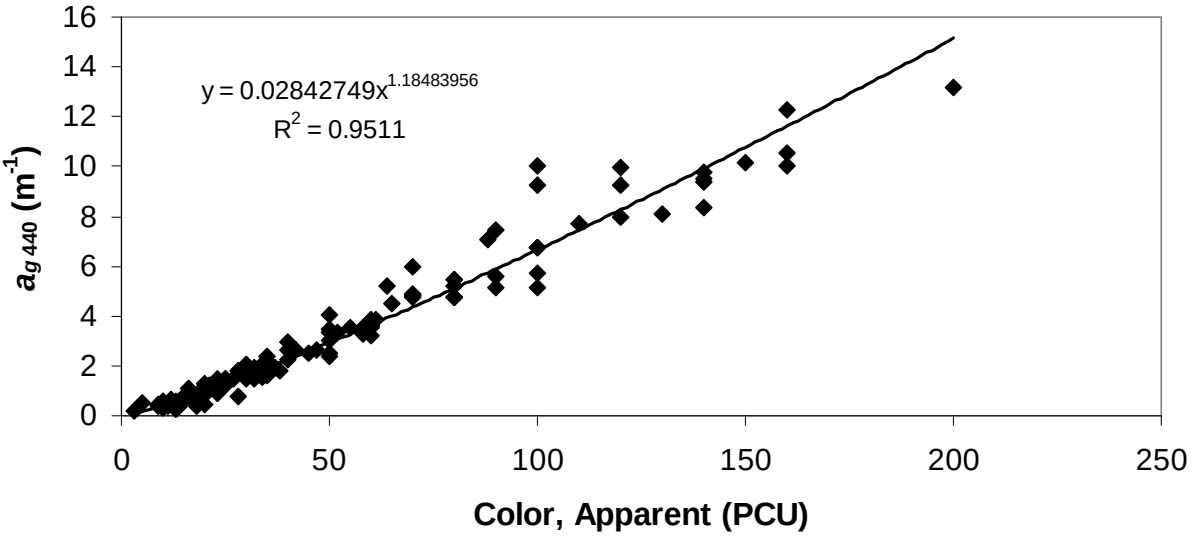

Figure 8. Observed a_{g440} as a function of apparent color, visually determined.

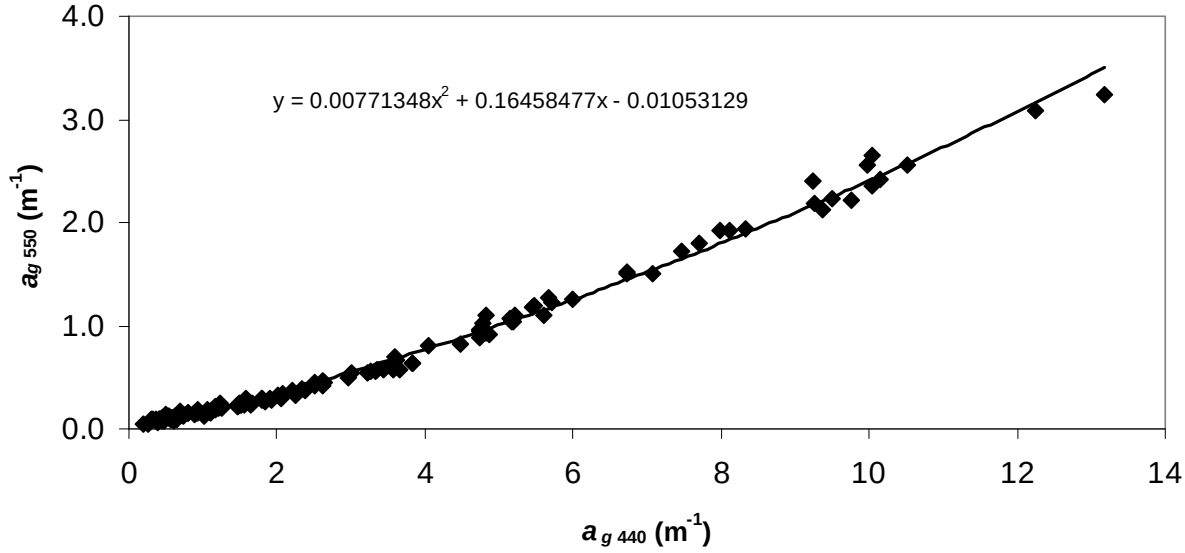

Figure 9. Observed a_{g550} as a function of observed a_{g440}

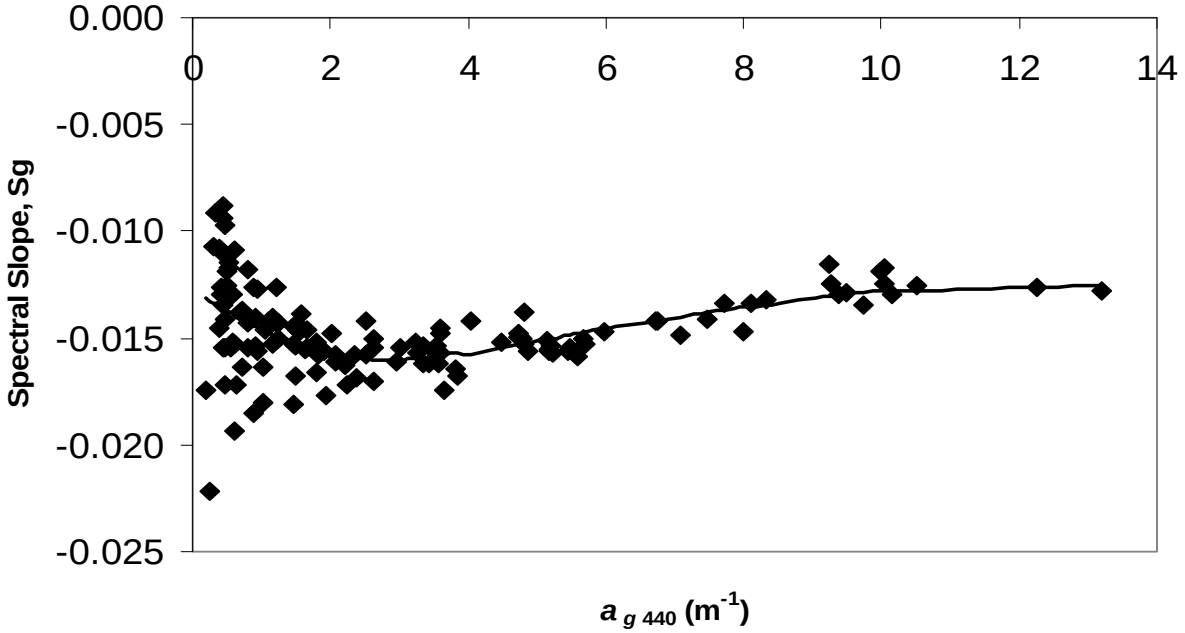

Figure 10. Spectral slope, S_g, 500-600 nm, as a function of observed a_{g440}.

Slopes were somewhat smaller than other literature references due to the longer wavelengths used for slope determination. Relationships between a_{g440} and Sg were determined from samples with a maximum a_{g440} of 13.1 m^{-1} (400 PCU for $Color_{PCU\text{-}Vis}$, and 260 PCU for $Color_{PCU\text{-}465}$), while samples to be modeled for status evaluations were as high as 33.7 m^{-1} (507 PCU for $Color_{PCU\text{-}Vis}$, and 375 PCU for $Color_{PCU\text{-}465}$). An amplification factor of 1.5 was used to minimize residuals across the range of a_{g440} observed.

2.3 SCATTERING

Scattering is strictly partitioned into that due to water and particulates as:

$$b = b_w + b_p \quad (15)$$

Scattering due to water alone varies roughly as λ^{-4} (Buitveld et al., 1994), but was a factor of 300-7000 times smaller than that due to particulates and was subsequently ignored for computational efficiency. Particulate scattering is less spectrally dependent than that due to water, and is primarily affected by particle size and refractive index. Scattering is reported to be best described as a direct function of turbidity (Morel and Gentili, 1991; Gallegos et al., 2008) with an inverse wavelength dependent term and scattering at a reference wavelength approximately equal to 0.92 to 1.1 times turbidity (Kirk, 1994). Other work has found varying exponents to the normalized wavelength term (Morel, 1973; Gallegos *et al*. 2009) ranging between 0.8 and 1.1, and occasionally dependent on color. The model was relatively insensitive to the precise scattering formula, but gave marginally better agreements of modeled K_{dPAR} with field measured K_{dPAR} using the formula as:

$$b(\lambda) = 1.1 * \text{Turbidity} * (555 / \lambda)^{0.8} \quad (16)$$

2.4 INSOLATION

Solar elevations were derived from the day of the year, solar declination, station latitude, and recorded time, and were adjusted for the time constant, the offset in minutes between the longitude of the station and the longitude of the eastern boundary of the start of the local time zone. Air masses, in Standard Atmospheres (SA; the path distance that sunlight travels for a given solar elevation relative to when the sun is directly overhead with SA=1.0), were computed from solar elevation, using an empirical adjustment for a curved rather than a plane-parallel atmosphere (Kasten and Young, 1989). Similar computations were used to calculate the maximum solar elevation (solar noon) for the sampling day.

Extraterrestrial spectral radiation (ASTM, 2003) was adjusted for the Earth-Sun distance for the day of the year (Kirk, 1994). "Global Tilt" values (spectral radiation from solar disk plus sky diffuse and diffuse reflected from ground on south facing surface tilted 37º from horizontal, under 1.5 Standard Atmospheres, SA; ASTM, 2003) were geometrically adjusted to normal values, and using Beer's Law, approximate atmospheric extinction coefficients (in units of SA^{-1}) were computed between adjusted global tilt and solar spectrum at top of atmosphere at the mean Earth-Sun distance (ASTM, 2003). Relevant spectra appear in Appendix C, Table C-3. Solar elevation, resulting SA, and derived atmospheric extinction coefficients were used to compute incident irradiance above the water surface. Reflectance at the air-water surface, a function of solar elevation (Austin, 1974; as shown in Kirk, 1994b) and considered spectrally flat, was removed resulting in irradiance just below the water surface, $I_{0\lambda}$. From the solar

elevation or zenith angle (Θ_a, 90º - solar elevation) in air, Snell's Law and the relative index of refraction between air and water was used to compute the zenith angle in water (Θ_w).

2.5 MODELED K_{DPAR}

For modeling, irradiance at depth, $I_{z\lambda}$, was computed for each wavelength from the individual spectral attenuation coefficients, $K_{d\lambda}$ as:

$$I_{z\lambda} = I_{0\lambda} * e^{(-Kd\lambda * z)} \quad (17)$$

Spectral irradiances were transformed to PAR measurements by integration of $I_{z\lambda}$ and $I_{0\lambda}$ over 400 to 700 nm. Modeled K_{dPAR} and %PAR were computed as:

$$\text{Modeled } K_{dPAR} = - ln\ (\Sigma\ [I_{z\lambda}] /\ \Sigma\ [I_{0\lambda}]\ ) / z \quad (18)$$

$$\%PAR = (\Sigma\ [I_{z\lambda}] /\ \Sigma\ [I_{0\lambda}]) * 100\% \quad (19)$$

As K_{dPAR} decreases with increasing depth interval due to differential absorption of selected wavelengths, when comparing modeled K_d with field observations made at selected depths, $I_{z\lambda}$ was computed at both the shallowest (z_1) and deepest (z_2) observation depths and the K_{dPAR} to compare to field observations was computed as:

$$\text{Modeled } K_{dPAR} = - ln\ (\Sigma\ [I_{z2\lambda}] /\ \Sigma\ [I_{z1\lambda}]\ ) / (z_2 - z_1) \quad (20)$$

3.0 MODEL CALIBRATION

3.1 POTENTIAL SOURCES OF VARIATION

Modeled and measured K_{dPAR} measurements often show extensive scatter in their relationship and a discussion of the contributing causes will assist the subsequent analysis of model calibration results. For field measurements, there are numerous subtleties in technique that effect data quality; making measurements at too shallow a depth for stable readings, allowing reflecting surfaces such as the boat hull to enhance upper sensor PAR readings, measuring over too short an integration time, or allowing reflection of light from sediments to enhance lower sensor readings.

When Kd is computed from PAR readings at multiple depths, the coefficient of determination, r^2, indicates the degree of fit. When evaluating data, criteria for a minimum r^2 (>0.95 for example) can be used to eliminate data with unusual depth profiles and suspect K_{dPAR} values. When two submersible sensors, separated by a known distance, are used to make a single pair of simultaneous readings, all r^2 values are 1.0, and there is no way to analytically exclude suspect readings.

On examination of light data from multiple depths, it is often the shallowest reading which does not conform to the expected linear decline in E_0 or Iz. Surface waves can serially focus and defocus surface light, creating moving "waves" of greater and lesser light intensity. The phenomena can be viewed as the lines of light moving across a shallow sandy bottom when in relatively clear waters, is more prevalent for shallower depths, and less apparent at deeper depths after multiple scattering produces a more uniform light field. (Making the shallowest readings at a 0.5 m minimum reduces this influence.) Longer integration times are an attempt to average the effect out and collect representative, mean PAR readings, but there could still be more light "spikes" during one integration period than during another. For a stationary subsurface point, the period of time with focused light is much shorter than that with de-focused light, with the distribution a function of the wave period and amplitude, and leading to a higher likelihood of depressed upper readings (reduced K_{dPAR}) relative to elevated readings (increased K_{dPAR}). If wave focusing is present, the effects will be greater in clear waters, and will also be evident as an increase in the variation of successive pairs of readings.

Diffuse attenuation coefficients such as K_d are considered an apparent optical property (AOP) and are influenced by the local angular distribution of radiance in addition to the inherent optical properties of absorption and scattering. A number of discrepancies between measured and modeled results may be attributed to the model simulating optically deep conditions and not accounting for changes in the subsurface angular distributions in light due to interactions with the bottom. Bottom reflectance of direct sunlight can increase the mean θ_w as direct sunlight reflects off of the sediments, which are typically considered to be lambertian reflectors radiating reflected light equally in all directions. An increase in measured K_{dPAR} relative to modeled values would result, but the bias between modeled and observed values K_d can be eliminated by excluding measurements made at shallow stations. Spherical sensors measuring E_0 from all directions are also subject to enhanced lower sensor readings from bottom reflectance, and could reduce measured K_{dPAR} relative to modeled values.

Other factors which effect the angular distribution of subsurface light are the result of varying proportions of direct sunlight and the remaining diffuse skylight from a blue or cloudy sky. The empirical model simulates the attenuation of direct sunlight only, or a sun in a "black" sky, while field measurements are influenced by the actual average angular distribution. During early morning measurements, when the sun is low on the horizon, a large proportion of illumination can be from the remaining hemisphere of the sky as diffuse light. The model will simulate the attenuation of direct sunlight with large θ_w and a subsequently much larger K_{dPAR} than will be measured in the field. Conversely, for midday observations under a completely cloudy sky, the model will simulate a low K_{dPAR} for a nearly vertical direct beam, while field measurements will be of a greater K_{dPAR} from a higher mean θ_w due to the predominance of diffuse illumination. Partially cloudy observations will have an intermediate influence. While field measurements of angular distribution can be made, these data are not typically available and cannot be directly incorporated in the optical model. Restricting the use of early morning data or data with very low irradiance values might limit the influence of these effects, but it should be kept in mind that together, the effects result in both positive and negative residuals, representing conditions that the model was not designed to incorporate.

Another contribution to variance between modeled and measured K_{dPAR} may be attributed to the character of turbidity. Water quality data (Figure 11) indicate that in addition to turbidity produced by phytoplankton, there can be mineral or detrital turbidity events where chlorophyll is negligible. The optical properties of both absorption and scattering undoubtedly differ for these various particle types. There are also variations in absorptive and scattering properties among phytoplankton species that cannot be retrieved from chlorophyll concentrations alone. Optical modeling calibrations have been formulated to fit a median type of particle, and variance between modeled and measured K_{dPAR} may result if particle types deviate substantially from the calibration data.

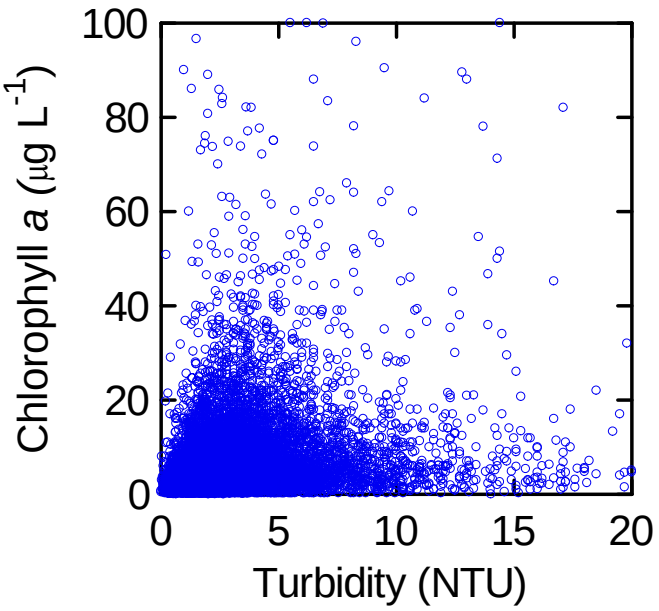

Figure 11. Relationship of chlorophyll and turbidity data.

Figure 12 summarizes the potential sources and relative effects of variation between modeled and observed $_{KdPAR}$. Although not explicitly included, typical analytical precision in determining water quality variables as well as field measurement precision will also contribute to variance between modeled and measured K_{dPAR} values. (It should be reemphasized that many of these biases are not measurement errors, but measurements under conditions that are not accounted for in the model.) Modeled results, however, have the advantage of providing K_d values that are a function of attenuating substances alone and do not vary based on cloud cover or time of sampling.

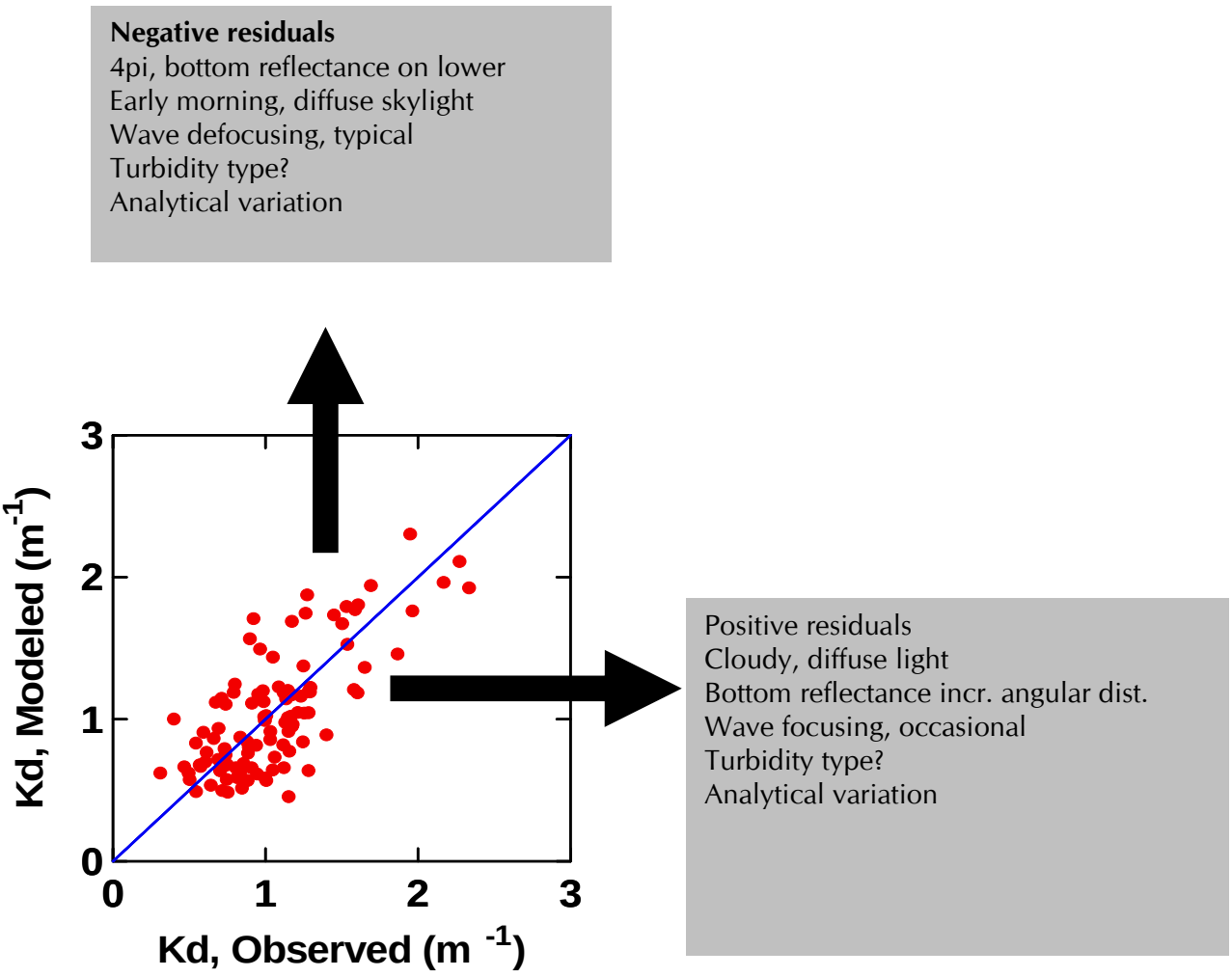

Figure 12. Summary of potential sources of variation between modeled and observed K_{dPAR}

3.2 CALIBRATION RESULTS

Model calibration consisted of exploration of the effects of the empirical parameters of g_1 and g_2, adjustments to the coefficients drawn from the literature to compute scattering from turbidity, and absorption-dependent adjustment of path amplification factors for the partial absorption coefficients. Residuals were also examined as a function of water quality parameters and other potential influences. Lastly calibration data were successively restricted to optimize the quality of field K_d and to minimize biases attributed to shallow waters and varying skylight as described above.

When examining model calibration results, it is also useful to keep in mind the uses to which the optical model will be applied. Designed to investigate the light climate at the deep edges of seagrass beds, model behavior at extremely low light levels (high K_{dPAR}) is not as important as accuracy at depths between 1-2 m and for light levels between ~10-40%PAR, where critical seagrass light requirements are anticipated to occur. Table 2 indicates that model accuracy of K_{dPAR} values less than ~1.6 m-1 are the most critical and that the lack of a full range of water quality data in the calibration data set is not as problematic as might be initially perceived.

Table 2. Illustration of the potential range of critical seagrass light requirements, example depths, and resulting needed K_{dPAR}.

%PAR	Depth (m)	Kd (m^{-1})
20	1.0	1.6
20	1.5	1.1
20	2.0	0.8
30	1.0	1.2
30	1.5	0.8
30	2.0	0.6
40	1.0	0.9
40	1.5	0.6
40	2.0	0.5

The slope of the calibration relationship (modeled K_{dPAR} as a function of observed) was expected to fall within 0.8-1.2, and was determined with a line of organic correlation (LOC), as errors were possible in both the *x* and *y* dimensions. In addition, it was desirable that the intercept of the LOC would be within ± 0.24 m^{-1}, the attenuation coefficient of pure water at the sampling depths.

Standard restrictions on calibration data were that r^2 of air corrected K_{dPAR} was greater than 0.95 and less than 1.00, that air corrected r^2 was greater than or equal to the r^2 of raw K_d, and that air corrected K_d was greater than 0.24 m^{-1}. The LOC slope was 0.853 (n=1005). Successive restrictions of the maximum depth to greater than 1.5 m (n=445) improved the LOC slope to a maximum of 0.982 and an intercept of -0.003. The reduction in outliers by restricting data to optically deep conditions (Figure 13) is apparent, and yet still maintains sufficient data for confidence in the critical range of K_{dPAR} less than 1.6 m^{-1}. Consistent with the LOC slope near 1.00, the median residual was 0.01 m^{-1}, and the median root mean square error was 0.15 m^{-1}. The median normalized root mean square error of the final calibration data was 15.9%. For those segments with data (all but DRB and ULB), there was no segregation by segment (Figure 14). Median residuals by segment were all less than 0.24 m^{-1}, the K_d of water alone, indicating a robust model effective for the 12 segments.

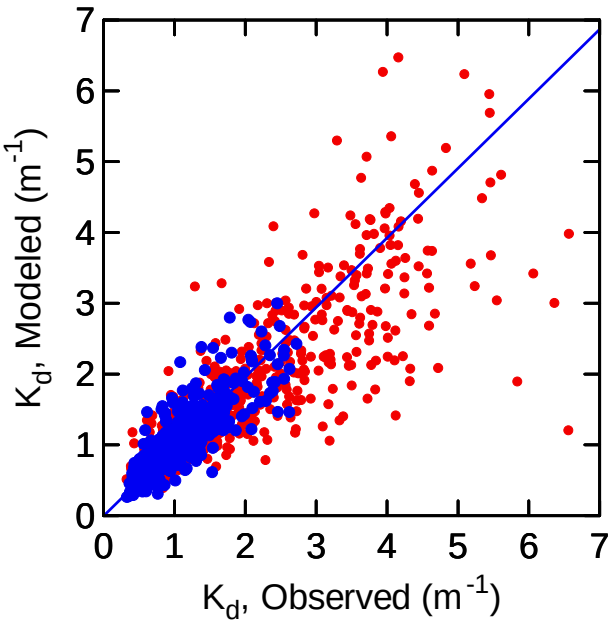

Figure 13. Modeled K_{dPAR} as a function of observed K_{dPAR} for standard restrictions (red; see text) and for standard restrictions plus maximum measurement depth greater than 1.5 m (blue, with LOC).

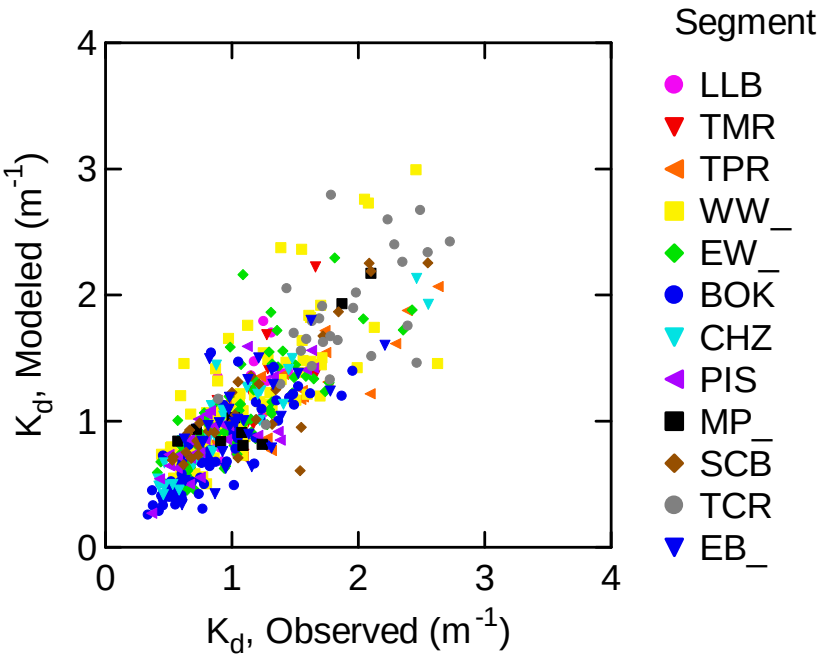

Figure 14. Modeled K_{dPAR} as a function of observed K_{dPAR} for standard restrictions and for maximum depth greater than 1.5 m.

For DRB and ULB, however, measurement techniques did not permit data restriction based on r^2, and so all observations were examined (Figure 15). Agreement between modeled and observed were again excellent, with an LOC slope of 1.005 and an intercept of 0.222 m^{-1}, although the increased scatter indicated some field measurements would have been censored had r^2 values been available. Residuals for all segments are summarized in Figure 16 where the increased scatter is again apparent for DRB and ULB, but overall model performance was acceptable with median residuals at or less than the attenuation coefficient of water alone.

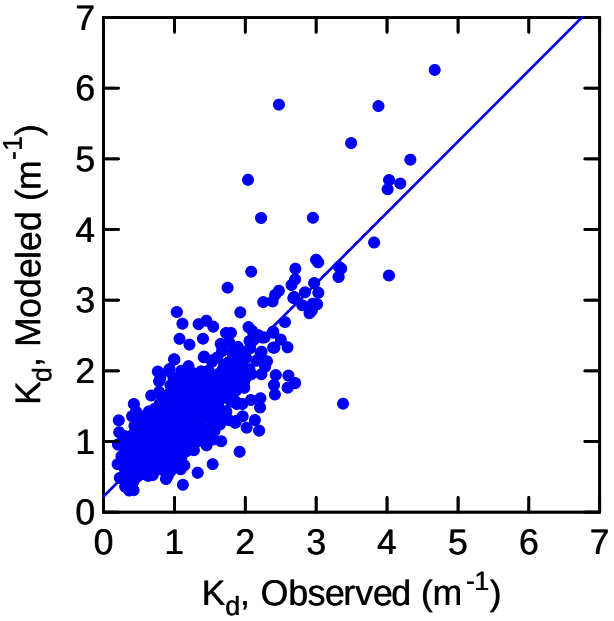

Figure 15. Modeled K_{dPAR} as a function of observed K_{dPAR} for all observations for DRB and ULB.

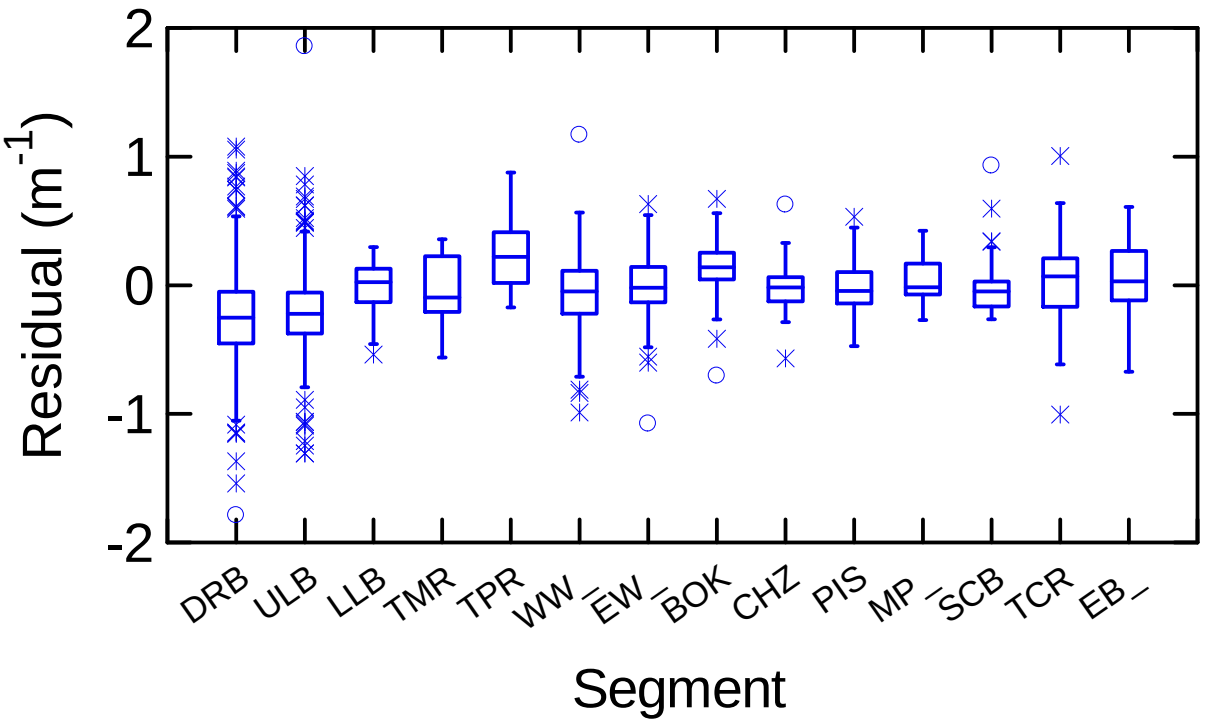

Figure 16. Residuals of observed less modeled Kd for all segments. Standard restrictions and maximum depth greater than 1.5 m for segments other than DRB and ULB; no restrictions for DRB and ULB.

3.3 DATA NEEDS FOR ENHANCED MODELING

Data for model calibration, both the specialized data needed to describe the spectral responses of color, chlorophyll and particulate absorption, and the concurrent observations of high quality field K_{dPAR} and water quality parameters, did not encompass as wide a concentration rage as was present in the time series of water quality data used to evaluate the reference period and other annual scores. As a result, the ability of the model to accurately represent these extremely high concentrations and high attenuation events is relatively uncertain. Addition of specialized data for high chlorophyll, turbidity, and color concentrations together with multi-depth K_{dPAR} determinations at deeper stations would allow model calibration to extend to the more extreme attenuations. The high attenuation events, however, represent the extremes of the distribution of K_{dPAR} with a given segment, as greater than 3.0 m^{-1} are generally beyond the 70^{th} percentiles established as target scores, would be unlikely to alter the distributional characteristics of an annual period relative to a reference period.

The particles contributing to turbidity were dominated by phytoplankton and detrital organics in the specialized data set used to characterize a_d. There are some segments, however, where

turbidity is occasionally dominated by mineral particulates resuspended as a result of onshore winds and beach resuspension. The resulting turbidity plumes are brought into the various passes on rising tides and have very different absorption properties than the detrital organics from further up-estuary. Additional absorption measurements on samples of this type would allow particulate absorption to be fit to a "mean" particle type and may improve the residuals in segments with access to the Gulf of Mexico. The types of particles could be further distinguished by total suspended solids (TSS) and volatile suspended solids (VSS) analyses, but model recalibration would need to be conducted to take advantage of the new analyses, and TSS and VSS would need to be incorporated into the CCHMN in the future.

The lack of PAR observations at more than two depths in Dona and Roberts Bays and Upper Lemon Bay limited the restrictions that could be placed on field K_{dPAR} data to ensure that the highest quality observations were used for model calibration. Review of all DRB and ULB data, however, indicated that the r^2 of modeled as a function of observed and the overall slope of the relationship was nearly identical between DRB and ULB data compared to the restricted data from the remaining segments. These data were accordingly used without restriction. Investigations of laboratory data and methods for spectrophotometric color would be helpful to confirm to confirm the variation in conversion of color in PCU determined at 465 nm to a_{g440}.

4.0 WATER CLARITY REPORTING TOOL

While mechanistic relationships between water quality conditions and the living resource requirements of seagrass are not fully understood, the preponderance of evidence suggests that water quality, explicitly water clarity, is a limiting factor in determining the depth distribution, and therefore areal extent, of seagrass. The most recent management efforts explicitly for seagrasses (JEI, 2010; JEI, 2011) proposed water clarity targets based on this assumption, and that improving water clarity will result in an increase in the areal extent of seagrasses given other factors are not limiting. Water clarity targets were identified that were relevant to the observed conditions affecting seagrass within each Harbor segment without explicitly identifying the light requirements of seagrass. A reference period was established when seagrasses delineation and water quality data were available and when seagrass areal loss or gain could be evaluated relative to baseline or historical conditions of seagrass coverage.

Within the selected reference period of 2003-2007, the cumulative distribution of ***measured*** light attenuation coefficients (K_{dPAR}) was generated for each Harbor segment (JEI, 2010). The 30^{th} and 70^{th} percentile values from the reference distribution were chosen as benchmark points from which to evaluate other years data. The benchmark points bracket water clarity conditions thought to be most representative of the light requirements of seagrass in each segment at the target depths established by CHNEP (Corbett, 2006). This project has replicated the reference period, frequency distribution, and annual evaluation approach but using ***modeled*** K_{dPAR} values. The methodology of the approach and the scoring method applied to "Protection" and "Restoration" segments is reproduced below from JEI (2010, 2011) for convenience.

4.1 SCORING METHOD

Janicki Environmental (2010, 2011) identified a method to derive annual, segment specific water clarity scores based on the frequency distribution of data collected under the CCHMN monitoring program. This section describes the application of that method to the modeled K_{dPAR}
From the spectrally explicit model. The binomial test (Wackerly et. al., 1996) is used as the tool to establish a scoring method to evaluate each year's water clarity data relative to the benchmark points, that is, the 30th and 70th percentile values from the reference period. For example:

- If more than 30% of the K_d measurements were below the benchmark with statistical significance (alpha=0.05), then the water clarity was considered to be improving and was assigned a value of positive 1.

- If less than 30% of the values were below the benchmark with statistical significance (alpha=0.05), then the water clarity was considered to be degrading and was assigned a value of negative 1.

- Otherwise the value was 0.

This scoring is performed on both endpoints (i.e. the 30th and 70th percentile). The sum of these scores is used to assess water clarity for each Harbor segment. The distribution of potential scores ranges from -2 to 2. To create the scores, all that needs to be known is the number of samples and the number of samples less than or equal to the criterion values for 30th and 70th percentile benchmarks.

Decision rules were also established specific to the categories of "Protection" or "Restoration".

- If the segment seagrass target was identified as a **Protection** target, then the water clarity target established will be a "hold the line" strategy to maintain ambient conditions experienced over the recent areal surveys.

- If the segment seagrass target was identified as a **Restoration** target, then the water clarity target will be an "Improvement" strategy measured as an "improving" trend in for light attenuation.

The tidal tributary seagrass targets including the Dona and Roberts Bays, Tidal Myakka, Tidal Peace, and Tidal Caloosahatchee Rivers were not to be considered as management targets for seagrass based on the subcommittee opinion that the influence of highly colored river waters reduced the ability to capture the bottom profile of these segments with aerial photography as well as the local observations of sparse but substantial coverage of seagrass in areas previously characterized by aerial photography as being devoid of seagrass. However, the tidal tributary

segments were assigned a restoration or protection water clarity target by CHNEP staff based on local expertise.
For the **Protection** targets the following grading system is used:

Green = score greater than -1	Stable
Yellow = score of -1 or less	Caution
Red = score of less than -1 for consecutive years	Declining

For the **Restoration** targets the following grading system is used:

Green = score greater than 1	Improving towards target
Yellow = score between -1 and 1	Caution
Red = score of less than -1	Declining

Based on this grading system, the Restoration targets have more stringent water quality criteria than the Protection targets. Stability in scores relative to the benchmark period is considered sufficient for the protection targets but not for the restoration targets. Therefore, scores between -1 and 1 are given a "caution" score. These scores can be related to changes in seagrass over time by either adding the scores between the biennial seagrass surveys, or evaluating each of the benchmark scores (i.e., the 30^{th} and 70^{th} percentile) separately. It should be noted that the binomial test used to score the water clarity data relies on the assumption that samples are independent and the design of the random stations of the CCHMN network conforms to this assumption. The test is also sensitive to changes in temporal sampling frequency that may bias the seasonal weighting of samples. The 30^{th} and 70^{th} percentiles of the reference period were develop with and applied to the current CCHMN sampling scheme which is monthly.

4.2 REFERENCE PERIOD AND FREQUENCY DISTRIBUTIONS

All water quality data for which values for color, corrected chlorophyll a, and turbidity were available were modeled using the calibrated optical model (electronic Appendix A). To compute reference frequency distributions and annual distributions, values of resulting modeled K_{dPAR} were then limited to those collected from the random stations of the CCHMN and the randomized stations of DRB and ULB. Density of each segment's selected data was reviewed to avoid bias from changing number of stations or missing sampling periods. The Tidal Caloosahatchee River segment changed from five monthly stations to three during 2006, but the three continued to extend over the entire segment. There were very few data from Matlacha Pass in 2003, and so the reference period for this segment was effectively 2004-2007. The fixed stations were excluded from the reference period and from the scoring analysis as they either varied in collection frequency over time or were not representative of the entire segment.) The resulting 30^{th} and 70^{th} percentiles of the 2003-2007 reference period appear in Table 3. An example of the distributions from which these values were drawn is illustrated in Figure 17 and appears for all segments in Appendix D.

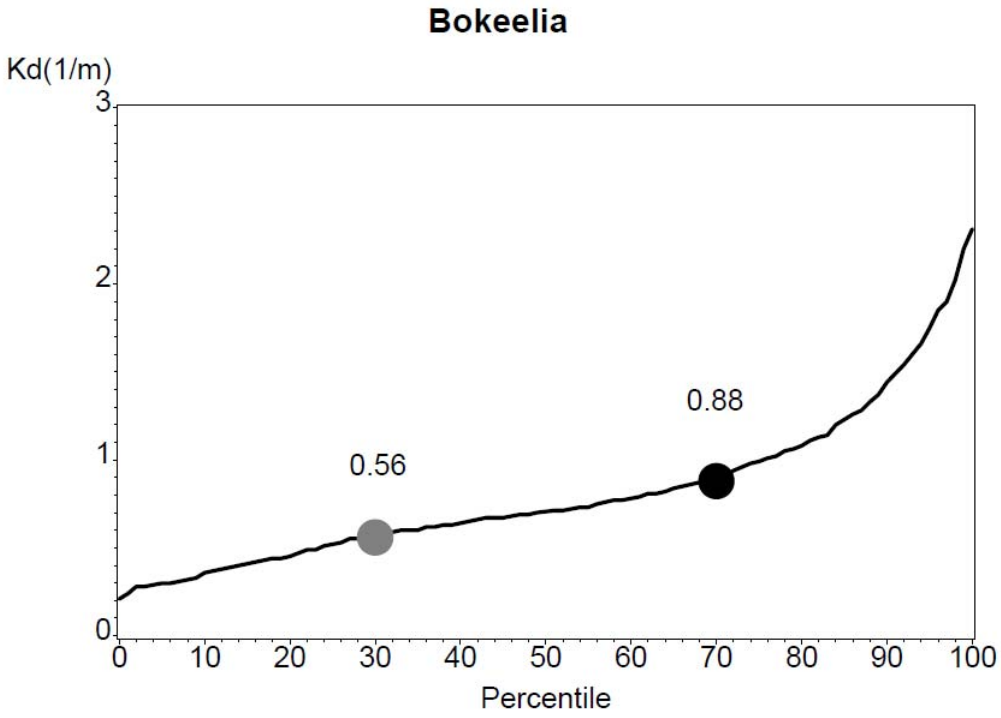

Figure 17. Example of the distribution of all modeled K_{dPAR} from the Bokeelia segment and the identification of the 30th and 70th percentiles.

Table 3. Selected percentiles of the frequency distribution of modeled K_{dPAR} from 2003-2007, by seagrass segment.

Segment	30th %-ile	70th %-ile
Dona and Roberts Bays*	0.90	1.35
Upper Lemon Bay	0.85	1.17
Lower Lemon Bay	0.75	1.13
Tidal Myakka River*	1.47	2.46
Tidal Peace River*	1.39	2.41
West Wall	0.87	1.40
East Wall	0.71	1.17
Cape Haze	0.74	1.06
Bokeelia	0.56	0.88
Pine Island Sound	0.71	0.98
Matlacha Pass	0.62	0.92
San Carlos Bay	0.57	0.91
Tidal Caloosahatchee River*	1.68	2.92
Estero Bay	0.96	1.39

4.3 ANNUAL SCORES

Annual scores were computed for each segment, and coded according to the decision rules described above. Scores were computed provided data were available in approximately nine of twelve months, but it should be kept in mind that the initial scores of each segment may be slightly biased by an incomplete year of water quality data. Table 4 illustrates the resulting scores and decision rule categories.

In addition to segment-specific performance, a number of region-wide trends were evident in the time series of scores. The years of 2001-2003 were often relatively decreased in water clarity, while 2007 was "Stable" or "Improving" in all segments. More recently, clarity declined in many segments in 2010. In 2011, there were some improvements over 2010. The segments of Upper Lemon Bay, Tidal Myakka River, Bokeelia, and Pine Island Sound were the segments which recorded the most stable or improving categories over the period of record, consistent with the large areas of seagrasses present in these regions. Application of a similar scoring technique to salinity may help determine the extent to which changes in annual scores are correlated with climatic variations.

Table 4. Results of Water Clarity Estimating Tool applied to water quality data from CCHMN random stations for each CHNEP Estuary Strata. Strata with seagrass restoration targets are shown on the left, in blue and strata with seagrass protection targets are shown on right, in black (Janicki, 2009). Note that the tool grading system is different for restoration vs. protection strata, to allow for earlier detection of trends in strata with restoration goals.

	CHNEP Strata with Seagrass RESTORATION Targets							
Year	Dona and Roberts Bays	Lower Lemon Bay	Tidal Peace River	West Wall	East Wall	Matlacha Pass	Tidal Caloosahatchee	Estero Bay
1998								
1999								
2000								
2001		-2	-2	-2	-2			
2002		-1	-1	-1	-2		-2	
2003	-2	-1	-2	-2	-2		-2	
2004	0	0	0	0	1	1	0	-1
2005	0	0	-1	-2	-2	-2	-2	0
2006	0	0	0	0	0	0	2	1
2007	2	1	2	2	2	2	2	2
2008	1	-1	0	1	1	0	1	-1
2009	0		-1	-1	-1	0	0	0
2010	-2		-1	1	1	-2	1	-2
2011	-1		0	-1	0	-2	1	-1

Strata with Seagrass PROTECTION Targets					
Upper Lemon Bay	Tidal Myakka River	Bokeelia	Cape Haze	Pine Island Sound	San Carlos Bay
-2					
-2					
-1					
0	-2		-2		
0	0	-2	-2		2
-1	-2	-2	-2		1
0	0	0	0	0	2
0	-1	-1	0	-1	-1
1	1	0	0	-1	-2
1	2	2	1	2	2
0	0	2	-1	2	0
1	0	1	-1	0	-1
-1	0	0	-1	0	-1
-1	-1	1	-2	0	-1

Grading system for Restoration targets:		
Green = score greater than 1	Improving	2
Yellow = score between -1 and 1	Caution	1
Red = score of less than -1	Caution	0
	Caution	-1
	Declining	-2

Grading system for Protection targets:		
Green = score greater than -1	Stable	2
	Stable	1
Yellow = score of -1 or less	Stable	0
	Caution	-1
Red = score of less than -1 for consec. yrs	**Caution /** Declining	-2

5.0 SUMMARY AND CONCLUSIONS

A spectrally explicit optical model was calibrated for the 14 seagrass management segments of Charlotte Harbor. Comparisons between modeled and observed K_{dPAR} were excellent overall and indicated a robust approach to computing water clarity in the ranges most relevant for seagrass growth. While results do not incorporate the short term variability in K_{dPAR} due to diurnal variations in cloud cover, sun angle, wave conditions or bottom reflectance, the modeled values are a more uniformly reliable indicator of water column clarity than the very difficult measurements of K_{dPAR} in very shallow systems.

The optical model provides an analytical approach to computing water clarity, K_{dPAR}, and %PAR, at predetermined depths and as a function of the water quality monitoring parameters, color, chlorophyll and turbidity. Scoring and the water clarity estimating tool were applied relative to a reference period and annual evaluations performed using data from the CCHMN probabilistic sampling design. The resulting simulations of water clarity were used to evaluate changes in water clarity relative to the 2003-2007 reference period. The water clarity estimation tool provides an important and easy to understand method of disseminating complex, non-linear attenuation processes to both public and managers alike. Routinely applied, both the model and the water clarity estimation tool will measure and report on estuarine conditions affecting key natural resources.

The use of the optical model is not limited to the periodic assessment of water clarity. A versatile tool, it can be applied to other sampling efforts within the Charlotte Harbor region. A highly relevant investigation would be the site-specific modeling with water quality data at the depths of seagrass transects to correlate modeled %PAR and the associated seagrass performance at multi-annual time scales.

6.0 REFERENCES

APHA. 2005. *Standard Methods for Examination of Water & Wastewater*: 21st Edition. American Public Health Association.

Arar, E. J., and G. B. Collins. 1997. *In vitro* determination of chlorophyll *a* and pheophytin *a* in marine and freshwater algae by fluorescence, p. 22. *In* N. E. R. Laboratory [ed.]. U.S. Environmental Protection Agency.

ASTM. 2003. ASTM Standard G173 - 03(2003), Standard Tables for Reference Solar Spectral Irradiances: Direct Normal and Hemispherical on 37° Tilted Surface. ASTM International, West Conshohocken, PA. DOI: 10.1520/G0173-03R12

Austin, R.W. 1974. The remote sensing of spectral radiance from below the ocean surface. In N.G. Jerlov & E.S. Nielssen, Eds. *Optical aspects of oceanography*, p. 317-44. London: Academic Press.

Biber, P.D., C.L. Gallegos and W.J. Kenworthy. 2008. Calibration of a bio-optical model in the North River, North Carolina (Albemarle – Pamlico Sound): A tool to evaluate water quality impacts on seagrasses. *Estuaries and Coasts* 31:177-191.

Bricaud, A., A. Morel, and L.Prieur. 1981. Absorption by dissolved organic matterof the sea (yellow substance) in the UV and visible domains. *Limnology and Oceanography* 26:43-53.

Bricaud, A., and D. Stramski. 1990. Spectral absorption coefficients of living phytoplankton and nonalgal biogenous matter: a comparison between the Peru upwelling area and the Sargasso Sea. *Limnology and Oceanography* 35: 562-582.

Buiteveld, H., J.H.M. Hakvoort and M. Donze, 1994: The optical properties of pure water. *Ocean Optics XII*, SPIE Vol. 2258: 174-183.

Butler, W. 1962. Absorption of light by turbid materials. *J. Opt. Soc. Am.* 52:292-299.

CHNEP. 2008. Committing to Our Future: A Comprehensive Conservation and Management Plan for the Greater Charlotte Harbor Watershed from Venice to Bonita Springs to Winter Haven. Charlotte Harbor National Estuary Program. Fort Myers, FL.

Cleveland, J.S. and A.D. Weidemann. 1993. Quantifying absorption by aquatic particles: A multiple scattering correction for glass-fiber filters. *Limnology and Oceanography* 38(6): 1321-1327.

Corbett, C. A. and J.A. Hale. 2006. Development of water quality targets for Charlotte Harbor, Florida using seagrass light requirements. *Florida Scientist* 69 (00S2): 36-50.

Corbett, C.A. 2006. Numeric Water Quality Targets for Lemon Bay, Charlotte Harbor and Estero Bay, Florida. Charlotte Harbor National Estuary Program Technical Report 06-3. Fort Myers, FL.

Dixon, L. K. 2000. Establishing Light Requirements for the Seagrass *Thalassia testudinum*: An example from Tampa Bay, Florida. *In* S. A. Bortone [ed.], *Seagrasses: Monitoring, Ecology, Phsiology, and Management*. Marine science series. CRC Press, Boca Raton, FL.

Dixon, L.K. 2014. Old Tampa Bay Integrated Model Development – Task 4 Optical Model Calibration Report. Mote Marine Laboratory Technical Report No. 1732. Sarasota, FL.

Dixon, L.K. and G.J. Kirkpatrick. 1995. Light attenuation with respect to seagrasses in Sarasota Bay, Florida. Mote Marine Laboratory Technical Report No. 407. Sarasota, FL.

Dixon, L.K. and G.J. Kirkpatrick. 1999. Causes of light attenuation with respect to seagrasses in upper and lower Charlotte Harbor. Final Report. Mote Marine Laboratory Technical Report No. 650. Sarasota, FL.

Dixon, L.K., E.R. Hall, and G.J. Kirkpatrick. 2010. A spectrally explicit optical model of attenuation for Charlotte Harbor seagrasses: Final report. Mote Marine Laboratory Technical Report No. 1460. Sarasota, FL.

Gallegos, C., Correll, D., and Pierce, J. (1990). Modeling spectral diffuse attenuation, adsorption, and scattering coefficients in a turbid estuary. *Limnology and Oceanography* 35: 1486-1502.

Gallegos, C.L. 2001. Calculating optical water quality targets to restore and protect submerged aquatic vegetation: Overcoming problems in partitioning the diffuse attenuation coefficient for photosynthetically active radiation. *Estuaries* 24: 381-397.

Gallegos, C.L. 1993. Determination of optical water quality requirements for growth of seagrasses in the Indian River near Ft. Pierce, FL, with emphasis on the impact of colored water discharges. Smithsonian Institution Office of Sponsored Projects Final Report to South Florida Water Management District, West Palm Beach, FL.

Gallegos, C.L. 1994. Refining habitat requirements of submersed aquatic vegetation: Role of optical models. *Estuaries*. 17(1B): 187-199.

Gallegos, C.L. 2005. Optical water quality of a black river estuary: The Lower St. Johns River, Florida, USA. *Estuarine, Coastal and Shelf Science* 63:57-72.

Gallegos, C.L., E.A. Lewis, and H.-C. Kim. 2006. Coupling suspended sediment dynamics and light penetration in the upper Chesapeake Bay. Smithsonian Environmental Research Center, Edgewater, MD. 36p.

Gallegos, C.L., R.J. Davies-Colley, and M. Gall. 2008. Optical closure in lakes with contrasting extremes of reflectance. *Limnology and Oceanography* 53(5): 2021-2034.

Gallegos, C.L., W.J. Kenworthy, P.D. Biber, and B.S. Wolfe. 2009. Underwater spectral energy distribution and seagrass depth limits along an optical water quality gradient. *Smithsonian Contributions to the Marine Sciences* 38: 359-367.

Greening, H. S. and A. Janicki. 2006. Toward Reversal of Eutrophic Conditions in a Subtropical Estuary: Water Quality and Seagrass Response to Nitrogen Loading Reductions in Tampa Bay, Florida, USA. *Environmental Management* 38(2): 163-178.

Janicki Environmental, Inc. 2010. Water quality target refinement project - Task 3: Water clarity target development. Interim Report 3. Prepared for Charlotte Harbor National Estuary Program, Ft. Myers, FL.

Janicki Environmental, Inc. 2011. Evaluation strategy and reporting tool for CHNEP water clarity targets – Task 3 Supplement. Prepared for Charlotte Harbor National Estuary Program, Ft. Myers, FL.

Janicki Environmental, Inc. 2009. Water Quality Targets Refinement Project Task 1: Harbor Segmentation Scheme. Prepared for Charlotte Harbor National Estuary Program, Ft. Myers, FL.

Janicki, A., M. Dema, and M. Wessel. 2009. Water Quality Target Refinement Project – Task 2: Seagrass target development. Interim Report 2. Prepared for Charlotte Harbor National Estuary Program, Ft. Myers, FL.

Johansson, J.O.R. 2007. Near-shore water quality and seagrass relationships in the upper portions of Tampa Bay, p. 43-48. *In* Corbett, C. (ed.), Colored dissolved organic matter (CDOM) workshop summary. Punta Gorda, Florida May 29-30, 2007.

Johansson, J.O.R. 2012. Application of a bio-optical model to determine light availability (PAR) at water depths required to reach the Tampa Bay seagrass restoration goal and at current depths of deep Tampa Bay seagrass meadows. Prepared for the Tampa Bay Estuary Program, St. Petersburg, FL.

Johansson, J.O.R., K.B. Hennenfent, W.M. Avery and J.J. Pacowta. 2009. Restoration of seagrass habitat in Tampa Bay using large manatee grass (*Syringodium filiform*e) sod units and a discussion of planting site sediment elevation dynamics, p. 153-163. *In* Cooper, S.T. (ed.), Proceedings, Tampa Bay Area Scientific Symposium, BASIS5, 20-23 October 2009, St. Petersburg, Fl. 538 p.

Kasten, F. and A.T. Young. 1989. Revised optical air mass tables and approximation formula. *Applied Optics* 28: 4735-4738.

Kirk, J. T. O. 1991. Volume scattering function, average cosines, and the underwater light field. *Limnology and Oceanography* 36: 455-467.

Kirk, J.T.O. 1994b. Characteristics of the light field in highly turbid waters : A Monte Carlo study. *Limnology and Oceanography* 39(3): 702-706.

Kirk, J.T.O. 1981. A Monte Carlo study of the nature of the underwater light field in, and the relationships between optical properties of turbid yellow waters. *Aust. J. Mar. Freshwater Res*. 32: 517–532.

Kirk, J.T.O. 1984. Dependence of relationship between inherent and apparent optical properties of water on solar altitude. *Limnology and Oceanography* 29: 350-356.

Kirk, J.T.O. 1994. *Light and Photosynthesis in Aquatic Ecosystems*. Second Edition. Cambridge University Press, Cambridge, MA.

Kishino, M., M. Takahashi, N. Okami and S. Ichimura. 1985. Estimation of the spectral absorption coefficients of phytoplankton in the sea. *Bull. Mar. Sci.* 37:634-642.

McPherson, B.F. and R.L. Miller. 1994. Causes of light attenuation in Tampa Bay and Charlotte Harbor, Southwestern Florida. *Water Resources Bulletin* V30(1): 43-53

Mobley, C.D. 1994. *Light and Water: Radiative Transfer in Natural Waters*. Academic Press.

Morel, A. 1973. Diffusion de la lumière par les eaux de mer; résultats expérimentaux et approche théorique, in *AGARD Lect. Ser.*, pp. 3.1.1.-3.1.76.

Morel, A. and B. Gentili. 1991. Diffuse reflectance of oceanic waters: Its dependence on sun angle as influenced by the molecular scattering contribution. *Applied Optics* 30: 4427-4438.

Mueller, J.L., Giulietta S. Fargion and Charles R. McClain, Editors. 2003. Ocean Optics Protocols For Satellite Ocean Color Sensor Validation, Revision 4, Volume IV: Inherent Optical Properties: Instruments, Characterizations, Field Measurements and Data Analysis Protocols NASA/TM-2003-211621/Rev4-Vol.IV, Goddard Space Flight Space Center, Greenbelt, Maryland 20771

Nelson, N. B., and C. Y. Robertson. 1993. Detrital spectral absorption: laboratory studies of visible light effects on phytodetritus absorption, bacterial spectral signal, and comparison to field measurements. *Journal of Marine Research* 51: 181-207.

Nelson, N. B., and C. Y. Robertson. 1993. Detrital spectral absorption: laboratory studies of visible light effects on phytodetritus absorption, bacterial spectral signal, and comparison to field measurements. *Journal of Marine Research* 51: 181-207.

Pope, R.M. and E. S. *Fry*. 1997. Absorption spectrum (380–700 nm) of pure water. II. Integrating cavity measurements, *Applied Optics*. 36:8710-8723.

Tomasko, D. A. and M. O. Hall. 1999. Productivity and biomass of the seagrass *Thalassia testudinum* along a gradient of freshwater influence in Charlotte Harbor, Florida. Estuaries 22(3A): 592-602.

Wackerly, D.D. W. Mendenhall and R.L. Scheeaffer. *Mathematical Statistics with Applications*. 5th Edition 1996. Wadsworth Publishing Company. Belmont California 94002.

Wessel, M.R., and C. Corbett. 2009. Assessing the Performance of an Optical Model Used in Setting Water Quality Targets in Lemon Bay, Charlotte Harbor and Estero Bay, FL. *Florida Scientist* 72(4): 367-385.

APPENDIX C

Table C-1. Spectral absorption coefficients of pure water (Pope and Fry, 1997).

nm	a_w (m^{-1})	nm	a_w (m^{-1})	nm	a_w (m^{-1})
400	0.00660	500	0.02040	600	0.2224
402	0.00590	502	0.02220	602	0.2431
404	0.00550	504	0.02460	604	0.2546
406	0.00520	506	0.02650	606	0.2602
408	0.00500	508	0.02870	608	0.2634
410	0.00470	510	0.03250	610	0.2644
412	0.00460	512	0.03640	612	0.2661
414	0.00450	514	0.03900	614	0.2673
416	0.00440	516	0.03980	616	0.2687
418	0.00440	518	0.04000	618	0.2715
420	0.00450	520	0.04090	620	0.2755
422	0.00470	522	0.04150	622	0.2802
424	0.00480	524	0.04160	624	0.2821
426	0.00480	526	0.04210	626	0.2863
428	0.00480	528	0.04290	628	0.2908
430	0.00490	530	0.04340	630	0.2916
432	0.00500	532	0.04450	632	0.2982
434	0.00520	534	0.04500	634	0.3005
436	0.00550	536	0.04570	636	0.3036
438	0.00590	538	0.04680	638	0.3083
440	0.00630	540	0.04740	640	0.3108
442	0.00680	542	0.04850	642	0.3202
444	0.00730	544	0.05020	644	0.3237
446	0.00780	546	0.05210	646	0.3288
448	0.00850	548	0.05420	648	0.3360
450	0.00920	550	0.05650	650	0.3400
452	0.00960	552	0.05890	652	0.3544
454	0.00970	554	0.05960	654	0.3655
456	0.00960	556	0.05990	656	0.3792
458	0.00960	558	0.06080	658	0.3970
460	0.00980	560	0.06190	660	0.4100
462	0.01000	562	0.06370	662	0.4219
464	0.01010	564	0.06400	664	0.4273
466	0.01010	566	0.06520	666	0.4319
468	0.01030	568	0.06770	668	0.4366
470	0.01060	570	0.06950	670	0.4390
472	0.01080	572	0.07250	672	0.4469
474	0.01120	574	0.07540	674	0.4474
476	0.01170	576	0.07960	676	0.4527
478	0.01220	578	0.08480	678	0.4623
480	0.01270	580	0.08960	680	0.4650
482	0.01300	582	0.09680	682	0.4755
484	0.01340	584	0.10540	684	0.4826
486	0.01390	586	0.11470	686	0.4918
488	0.01450	588	0.12440	688	0.5048
490	0.01500	590	0.13510	690	0.5160
492	0.01600	592	0.14840	692	0.5336
494	0.01680	594	0.16040	694	0.5498
496	0.01800	596	0.17610	696	0.5713
498	0.01940	598	0.19840	698	0.5985
				700	0.6240

Table C-2. Coefficients for spectral modeling of a_{ph} in the form of $a_{ph} = C * Chl^{B}$.

nm	C	B	nm	C	B	nm	C	B
400	0.05284	0.60834	500	0.03642	0.64511	600	0.00792	0.72275
402	0.05315	0.61363	502	0.03527	0.64194	602	0.00753	0.74533
404	0.05310	0.61951	504	0.03443	0.63823	604	0.00787	0.72891
406	0.05481	0.61609	506	0.03303	0.64188	606	0.00780	0.74366
408	0.05737	0.60401	508	0.03147	0.64628	608	0.00794	0.75143
410	0.05790	0.60938	510	0.03101	0.63841	610	0.00837	0.74534
412	0.05996	0.60223	512	0.02969	0.63689	612	0.00825	0.76179
414	0.06038	0.60636	514	0.02838	0.64248	614	0.00853	0.76311
416	0.06146	0.60351	516	0.02698	0.64852	616	0.00800	0.80068
418	0.06116	0.61007	518	0.02683	0.63089	618	0.00888	0.76801
420	0.06223	0.60627	520	0.02620	0.62709	620	0.00891	0.77859
422	0.06250	0.60571	522	0.02437	0.64017	622	0.00876	0.78589
424	0.06131	0.61221	524	0.02331	0.64218	624	0.00898	0.78133
426	0.06305	0.60502	526	0.02220	0.64944	626	0.00849	0.80228
428	0.06177	0.61859	528	0.02173	0.64502	628	0.00897	0.78526
430	0.06281	0.61861	530	0.02147	0.63298	630	0.00904	0.78457
432	0.06461	0.61274	532	0.02011	0.64741	632	0.00884	0.79758
434	0.06480	0.61587	534	0.01974	0.64556	634	0.00928	0.77647
436	0.06544	0.61141	536	0.01839	0.66277	636	0.00875	0.79565
438	0.06493	0.61672	538	0.01813	0.65607	638	0.00846	0.80164
440	0.06590	0.60878	540	0.01728	0.65933	640	0.00858	0.79086
442	0.06360	0.61791	542	0.01717	0.65060	642	0.00860	0.77626
444	0.06260	0.61517	544	0.01672	0.64293	644	0.00833	0.78965
446	0.06177	0.61031	546	0.01582	0.65558	646	0.00882	0.75530
448	0.06020	0.61123	548	0.01614	0.63198	648	0.00746	0.82390
450	0.05793	0.61462	550	0.01548	0.63498	650	0.00770	0.81246
452	0.05829	0.60172	552	0.01433	0.64667	652	0.00803	0.80349
454	0.05584	0.61482	554	0.01395	0.64242	654	0.00860	0.78809
456	0.05547	0.61219	556	0.01356	0.64609	656	0.00915	0.79696
458	0.05524	0.61047	558	0.01387	0.61832	658	0.00967	0.81569
460	0.05486	0.60988	560	0.01314	0.62297	660	0.01060	0.82297
462	0.05248	0.62518	562	0.01208	0.64382	662	0.01168	0.83453
464	0.05276	0.61877	564	0.01135	0.66409	664	0.01437	0.79646
466	0.05175	0.62231	566	0.01177	0.63993	666	0.01571	0.80390
468	0.05086	0.62159	568	0.01043	0.68109	668	0.01681	0.81317
470	0.04952	0.62507	570	0.01007	0.68825	670	0.01887	0.79287
472	0.04899	0.61960	572	0.01085	0.65623	672	0.02017	0.78515
474	0.04727	0.62692	574	0.00973	0.68927	674	0.02065	0.78858
476	0.04594	0.62808	576	0.01031	0.66540	676	0.02189	0.77315
478	0.04641	0.61552	578	0.00962	0.68063	678	0.02014	0.78797
480	0.04520	0.61969	580	0.01000	0.66984	680	0.01883	0.79407
482	0.04489	0.61881	582	0.00838	0.72838	682	0.01701	0.80508
484	0.04351	0.62643	584	0.00907	0.70170	684	0.01491	0.80933
486	0.04436	0.61479	586	0.00816	0.73309	686	0.01237	0.82490
488	0.04369	0.61556	588	0.00901	0.70488	688	0.01030	0.81779
490	0.04299	0.61857	590	0.00861	0.71615	690	0.00838	0.81380
492	0.04123	0.63077	592	0.00786	0.75104	692	0.00690	0.79360
494	0.04012	0.63492	594	0.00777	0.74425	694	0.00512	0.81613
496	0.03970	0.62919	596	0.00765	0.74304	696	0.00435	0.77669
498	0.03868	0.63051	598	0.00735	0.75309	698	0.00339	0.78831
						700	0.00160	1.03518

Table C-3. Atmospheric extinction coefficients and extraterrestrial radiation (solar spectrum at top of atmosphere) at mean Earth-Sun distance.

(nm)	Atmosph. Extinct. Coeff (SA^{-1})	I_{ta} ($W\ m^{-2}\ nm^{-1}$)	(nm)	Atmosph. Extinct. Coeff (SA^{-1})	I_{ta} ($W\ m^{-2}\ nm^{-1}$)	(nm)	Atmosph. Extinct. Coeff (SA^{-1})	I_{ta} ($W\ m^{-2}\ nm^{-1}$)
400	0.45270	1.68850	500	0.22600	1.91600	600	0.17880	1.77000
402	0.44420	1.81400	502	0.22650	1.86000	602	0.17560	1.71500
404	0.43660	1.76300	504	0.23280	1.83300	604	0.17420	1.77900
406	0.42900	1.66600	506	0.22600	2.02500	606	0.17050	1.75800
408	0.42210	1.69900	508	0.22240	1.88000	608	0.16590	1.75100
410	0.41500	1.53700	510	0.21870	1.91000	610	0.16330	1.72400
412	0.40740	1.81600	512	0.21540	1.98900	612	0.16130	1.73600
414	0.40120	1.71440	514	0.21280	1.82400	614	0.15940	1.65500
416	0.39380	1.81500	516	0.21120	1.89100	616	0.15660	1.66400
418	0.38780	1.68500	518	0.20930	1.75900	618	0.15520	1.70200
420	0.38180	1.59900	520	0.20830	1.86000	620	0.15520	1.71100
422	0.37570	1.78200	522	0.20750	1.91500	622	0.16360	1.67840
424	0.37000	1.70800	524	0.20680	1.94100	624	0.16580	1.66700
426	0.36310	1.69900	526	0.20690	1.87400	626	0.16000	1.64000
428	0.35830	1.65100	528	0.20760	1.88000	628	0.19870	1.69300
430	0.35190	1.21200	530	0.20740	1.89200	630	0.17360	1.66500
432	0.34650	1.82200	532	0.20640	1.95800	632	0.15690	1.59010
434	0.34170	1.56000	534	0.20450	1.86900	634	0.14560	1.63700
436	0.33650	1.86800	536	0.20250	1.97400	636	0.14150	1.60930
438	0.33050	1.66300	538	0.20030	1.91300	638	0.13730	1.66500
440	0.32690	1.83000	540	0.19920	1.80000	640	0.13300	1.61300
442	0.32150	1.92200	542	0.20030	1.88800	642	0.12960	1.60900
444	0.31770	1.89410	544	0.19880	1.91900	644	0.12760	1.61400
446	0.31320	1.75570	546	0.19940	1.86090	646	0.13230	1.59100
448	0.30930	2.01400	548	0.19690	1.82600	648	0.14600	1.60200
450	0.30310	2.06900	550	0.19460	1.86300	650	0.13100	1.52600
452	0.29900	2.04700	552	0.19300	1.89600	652	0.14490	1.59100
454	0.29430	2.01800	554	0.19250	1.87800	654	0.12510	1.57500
456	0.29050	2.06300	556	0.19230	1.85700	656	0.12710	1.32330
458	0.28770	2.03200	558	0.19280	1.85300	658	0.12370	1.53900
460	0.28430	1.99730	560	0.19290	1.78600	660	0.12510	1.55800
462	0.28010	2.07800	562	0.19310	1.80100	662	0.13860	1.57100
464	0.27650	2.01500	564	0.19390	1.83600	664	0.12450	1.55400
466	0.27170	2.02100	566	0.19450	1.75000	666	0.11380	1.55500
468	0.26930	2.01200	568	0.19780	1.85900	668	0.10770	1.53480
470	0.26670	1.93900	570	0.20220	1.82800	670	0.10510	1.53400
472	0.26420	2.07000	572	0.20340	1.87200	672	0.10340	1.50600
474	0.26290	2.01200	574	0.20410	1.87300	674	0.10170	1.51300
476	0.26320	2.01200	576	0.20470	1.81800	676	0.10030	1.51500
478	0.26070	2.08600	578	0.20170	1.79900	678	0.09930	1.50700
480	0.25560	2.06800	580	0.19370	1.83400	680	0.09810	1.49400
482	0.25020	2.06230	582	0.18670	1.85200	682	0.09700	1.49300
484	0.24590	1.98900	584	0.18190	1.85400	684	0.09640	1.46600
486	0.24240	1.60100	586	0.18050	1.79200	686	0.09590	1.43300
488	0.23950	1.93500	588	0.19150	1.82100	688	0.23390	1.47600
490	0.23710	2.03200	590	0.21060	1.72180	690	0.20010	1.47900
492	0.23400	1.85600	592	0.20480	1.78800	692	0.14260	1.45400
494	0.23170	1.93390	594	0.19860	1.78900	694	0.15560	1.45700
496	0.22960	1.94900	596	0.18940	1.79600	696	0.13730	1.44200
498	0.22730	1.92400	598	0.18640	1.77200	698	0.10020	1.41700
						700	0.12090	1.42200

APPENDIX D

CUMULATIVE DISTRIBUTION CURVES OF MODELED K_{dPAR}, 2003-2007

Dona and Roberts Bays

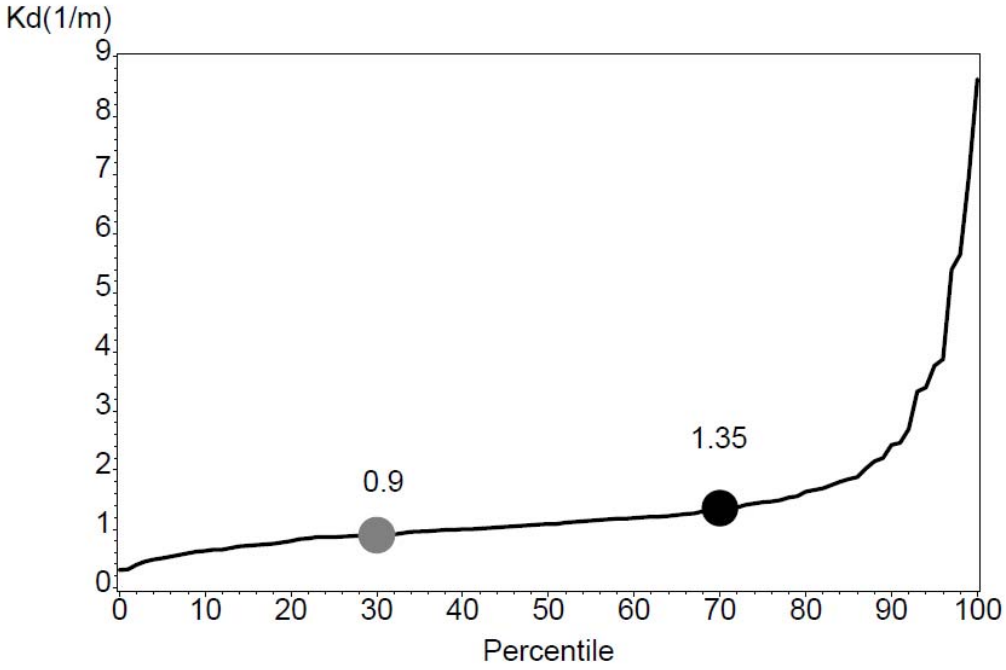

Upper Lemon Bay

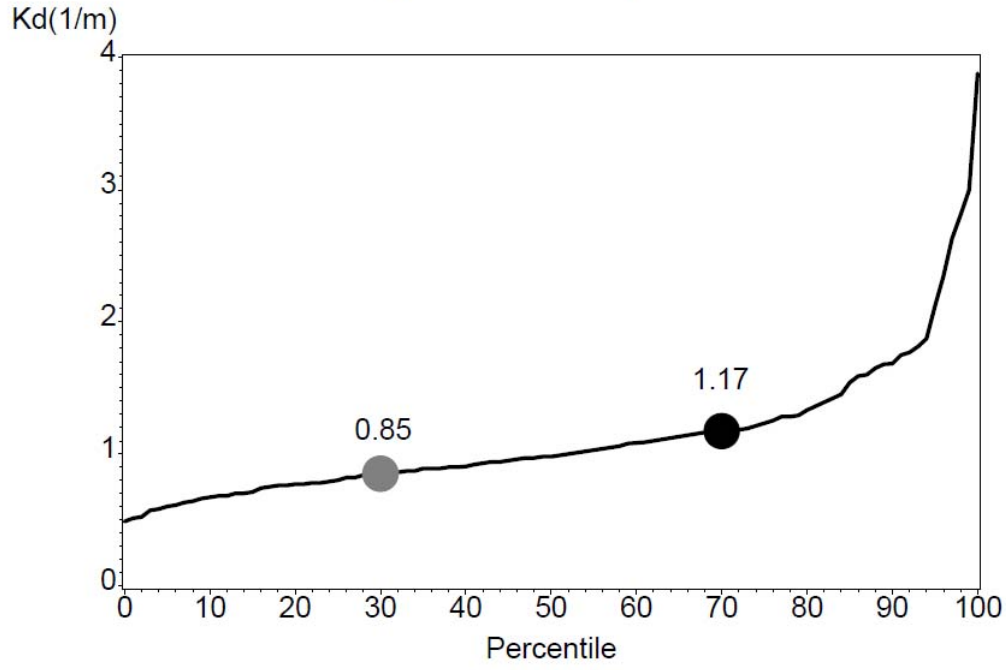

Lower Lemon Bay

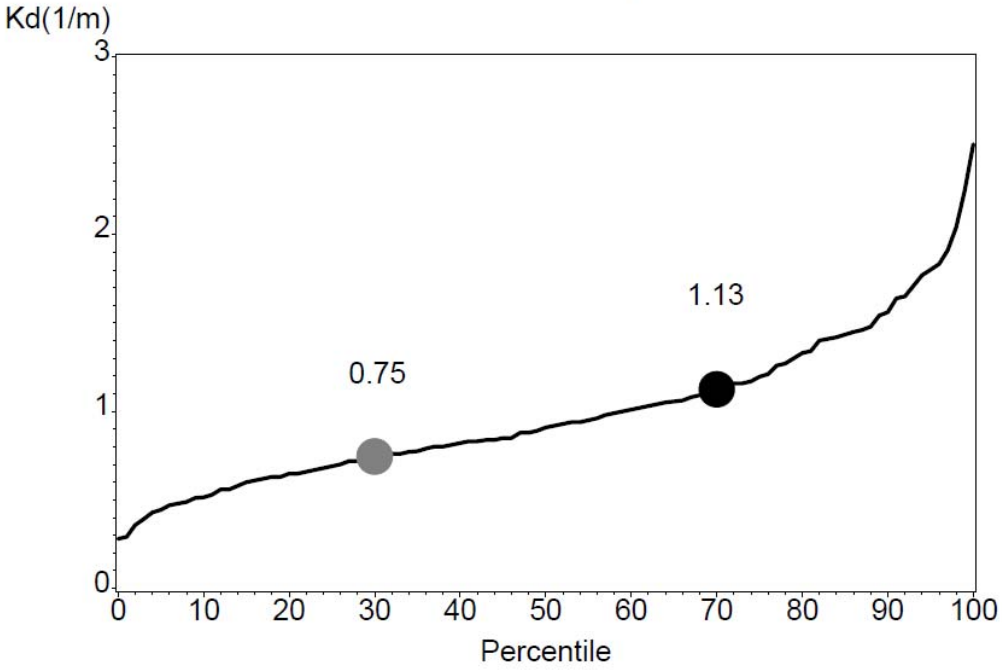

Tidal Myakka River

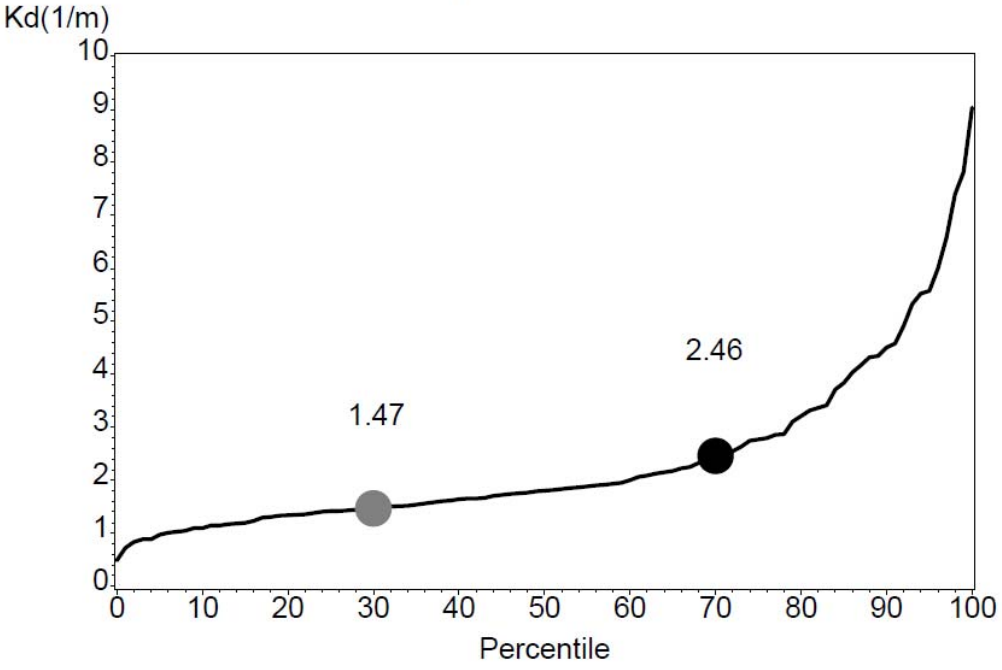

Tidal Peace River

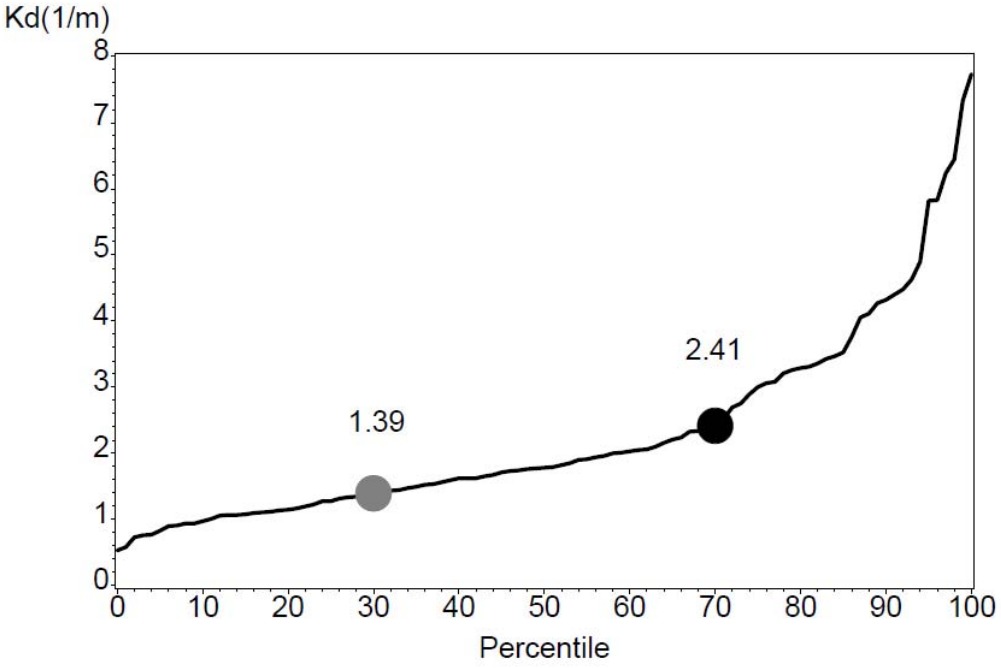

West Wall

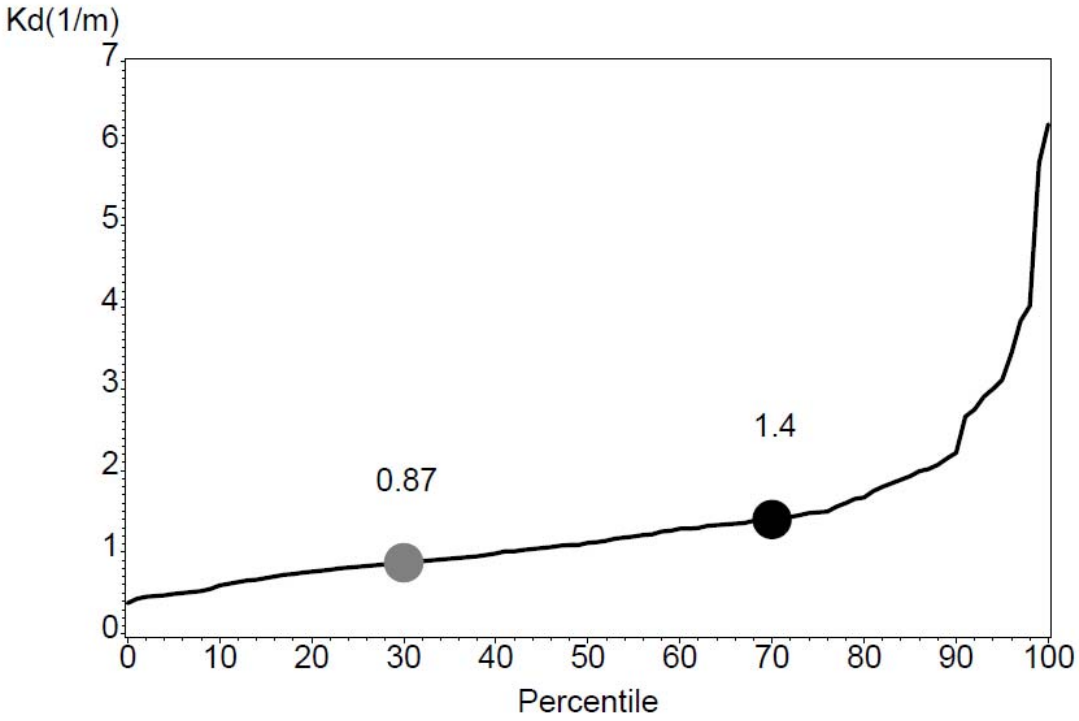

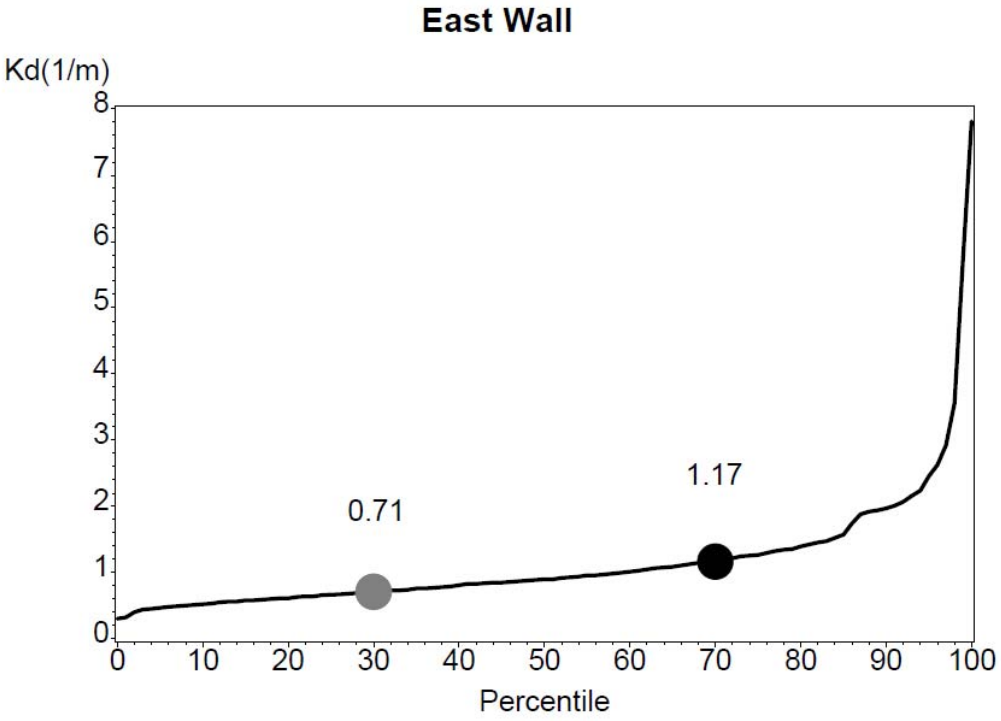
East Wall
Kd(1/m)
8
7
6
5
4
3
2
1
0
0.71
1.17
0
10
20
30
40
50
60
70
80
90
100
Percentile

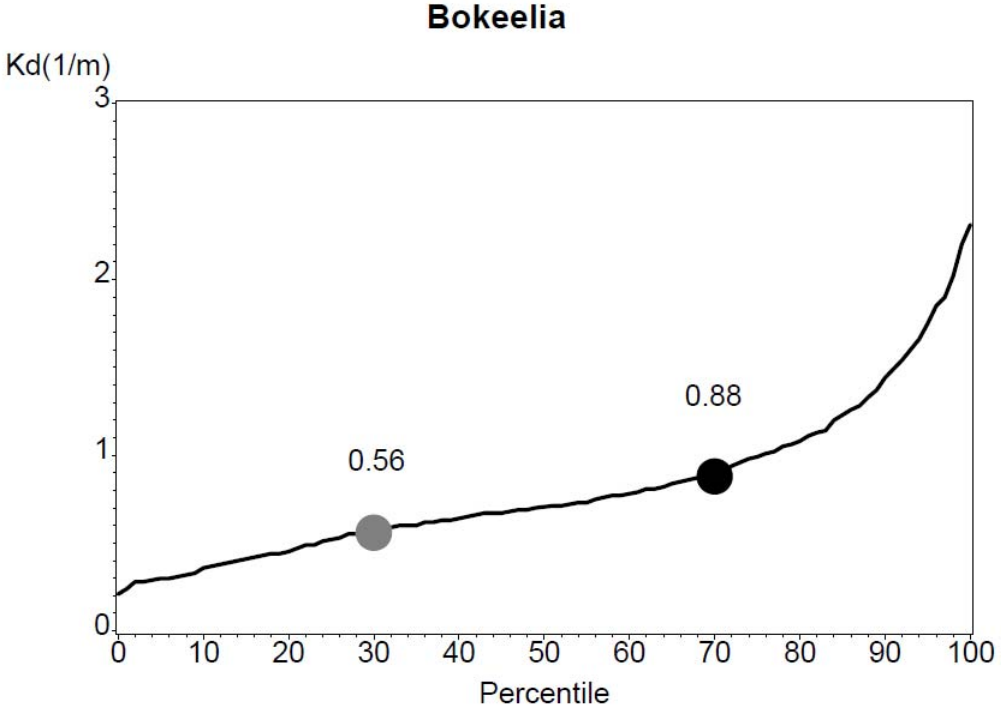
Bokeelia
Kd(1/m)
3
2
1
0
0.56
0.88
0
10
20
30
40
50
60
70
80
90
100
Percentile

Cape Haze

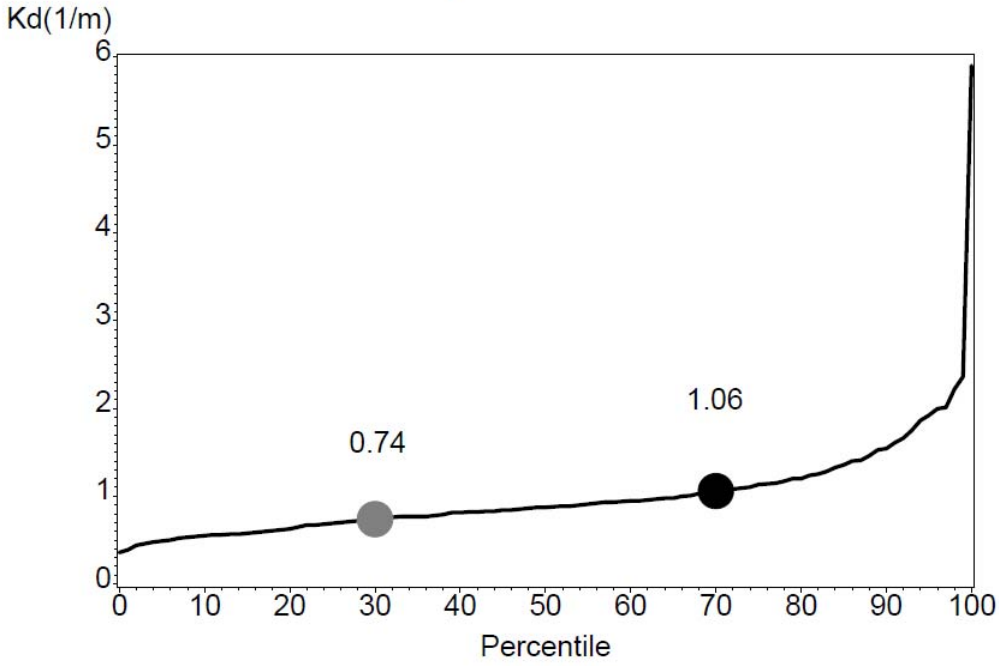

Matlacha Pass

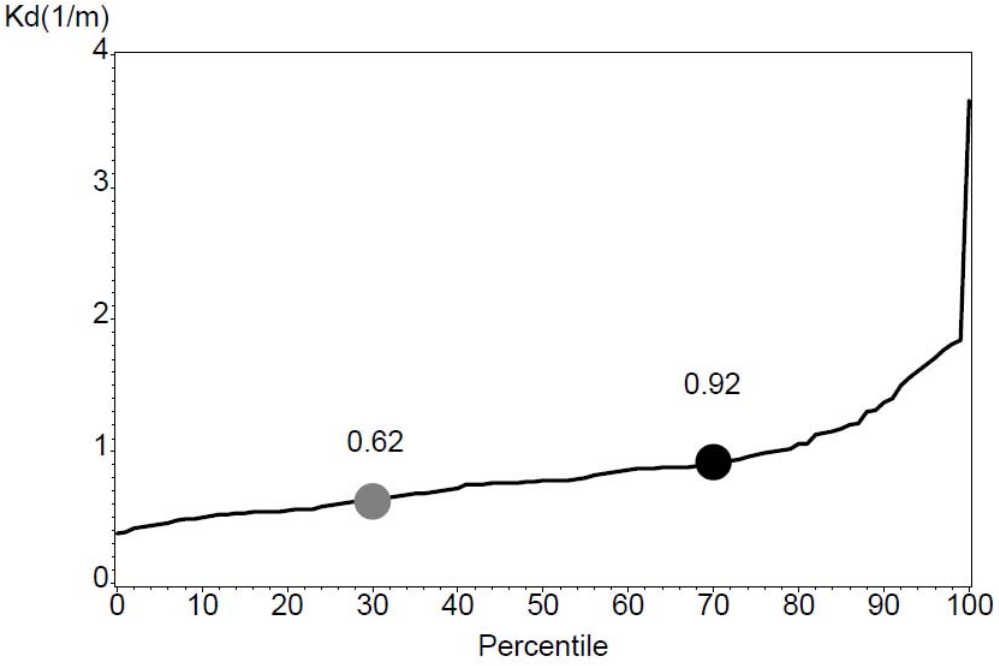

Pine Island Sound

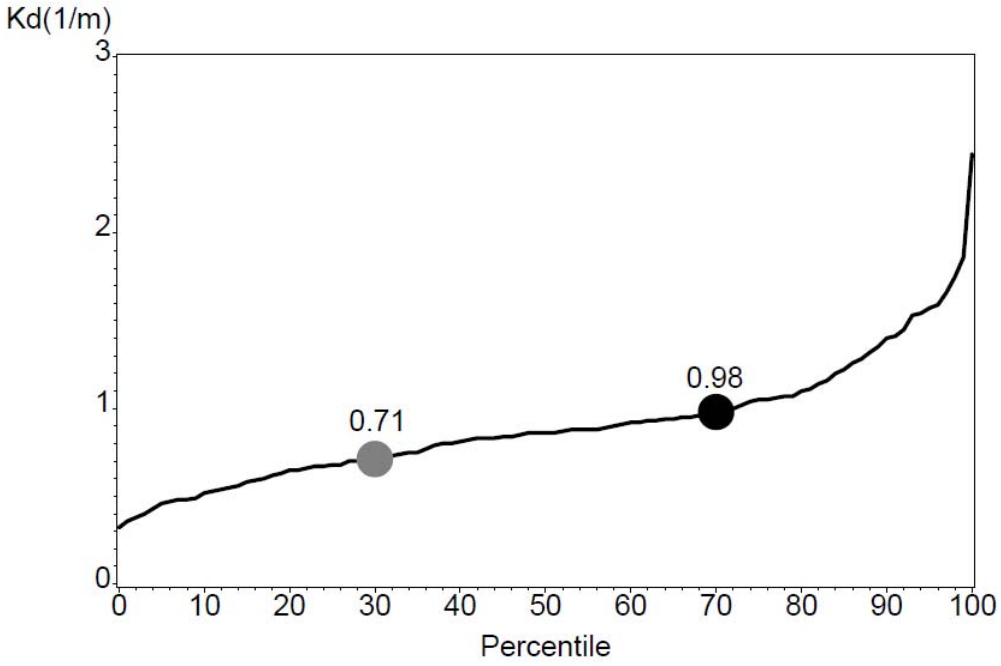

Tidal Caloosahatchee River

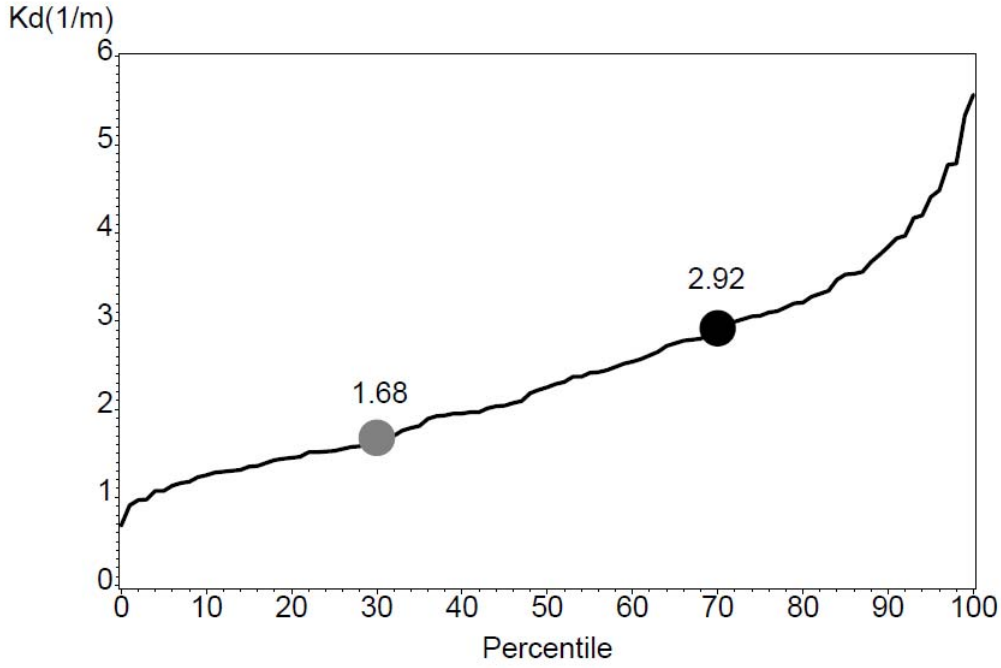

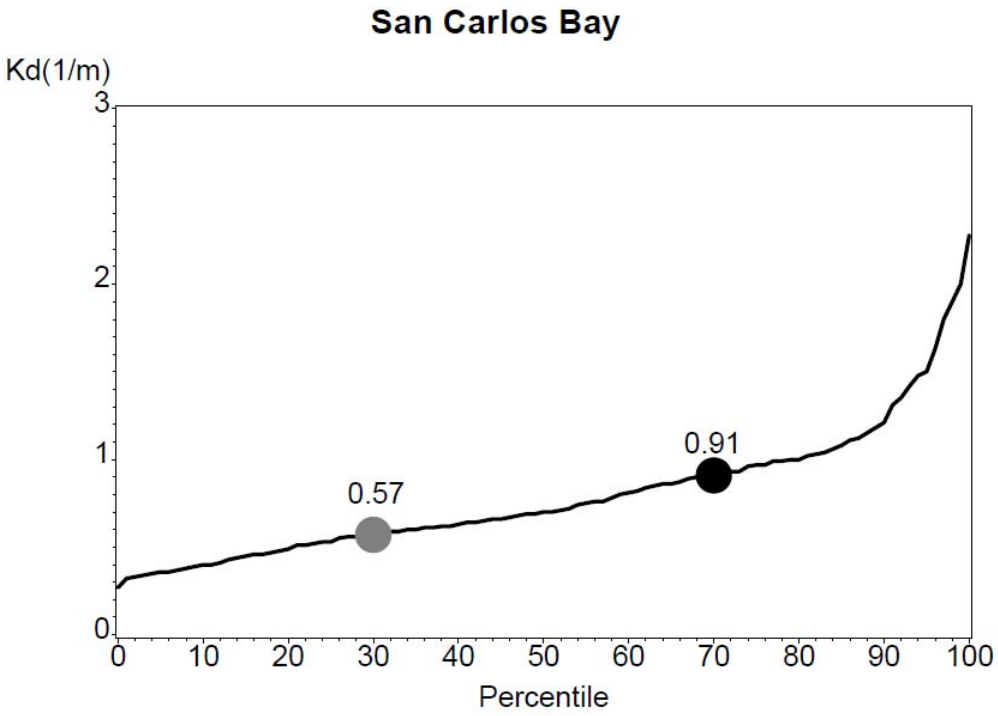
San Carlos Bay
Kd(1/m)
3
2
1
0
0.91
0.57
0 10 20 30 40 50 60 70 80 90 100
Percentile

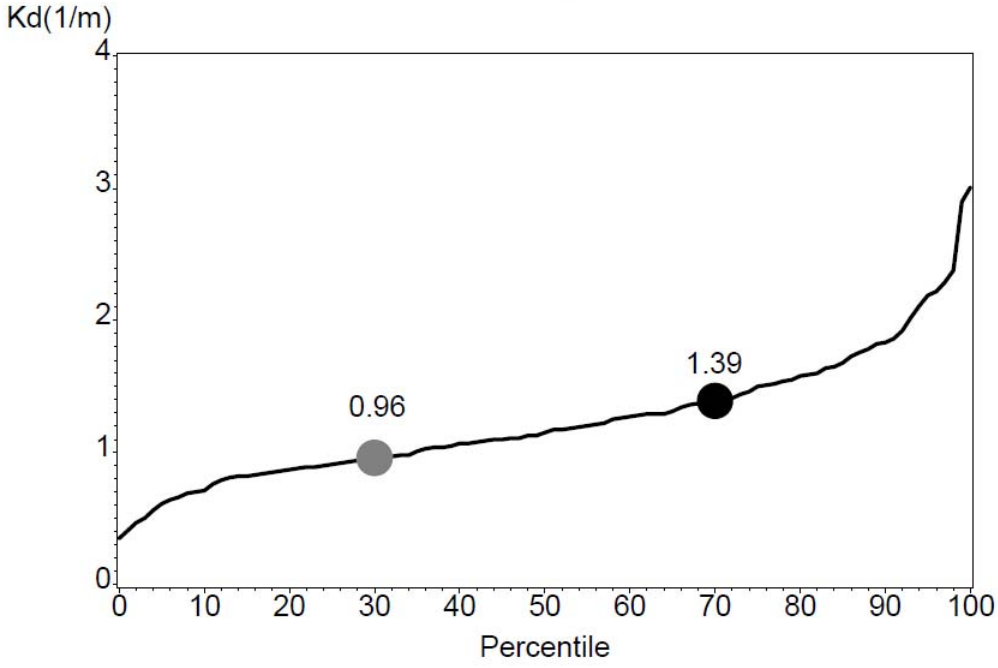
Estero Bay
Kd(1/m)
4
3
2
1
0
1.39
0.96
0 10 20 30 40 50 60 70 80 90 100
Percentile